most common genotype groups in Japanese population. Each of the three age-matched and biopsy site-matched samples from c.1714G>C homozygous group and c.1714G>C/c.527A>T compound heterozygous group was compared. Muscle samples were taken from biceps brachii and frozen with isopentane cooled in liquid nitrogen. Serial frozen sections of 10 μm were stained using a set of histochemical methods including haematoxylin-eosin and modified Gomori trichrome.

Statistical analysis

Statistics were calculated using GraphPad Prism 5 software (GraphPad Software, La Jolla, California, USA). Between-group comparison for clinical data was performed using one-way analysis of variance with Dunnett's post-test. All values are expressed as means±SD. We performed two-sided tests with a $p<0.05$ level of significance.

RESULTS

Mutation profile

We identified homozygous or compound heterozygous *GNE* mutations in all 212 patients (see online supplement 1). In total, 63 different mutations were found including 50 missense mutations, 2 nonsense mutations, 1 insertion, 4 deletions, 5 intronic mutations and 1 single exon deletion (figure 1). Twenty-five novel mutations were identified including 17 missense mutations, 4 small deletions, 3 intronic mutations and 1 single exon deletion (figure 1, see online supplement).

Twenty-one mutations were found to be shared between two or more unrelated families. The three mutations occurring most frequently in the Japanese population were c.1714G>C (p.Val572Leu), c.527A>T (p.Asp176Val) and c.38G>C (p.Cys13Ser); these comprised 48.3%, 22.4% and 3.5%, respectively, of the total number of alleles examined (table 1).

Table 1 Allele frequency for GNE mutations in 212 Japanese GNE myopathy patients

	Allele frequency
Mutation type	
Missense	402 (94.8%)
Nonsense	3 (0.7%)
Insertion	1 (0.2%)
Small deletion	4 (0.9%)
Single exon deletion	2 (0.5%)
Intron	12 (2.8%)
Three most common mutations	
c.1765G>C (p.Val572Leu)	205 (48.3%)
c.578A>T (p.Asp176Val)	95 (22.4%)
c.38G>C (p.Cys13Ser)	15 (3.5%)
Total alleles	424

Genotype–phenotype correlations

The mean age of genetic analysis was 41.6±14.1 years (n=212), and the mean age of symptom onset based on the data available was 28.4±10.2 years (n=195). The earliest onset age was 10 and the latest was 61 years old in our cohort. Thirty-six among 154 patients (23.4%) were full-time wheelchair users at the point of genetic diagnosis with the average age at loss of ambulation being 36.8±11.3 years (n=36). The youngest wheelchair-bound age was 19, and the oldest ambulant age was 78. To investigate genotype–phenotype correlations in the major *GNE* mutations of Japanese population, we compared the age at symptom onset and loss of ambulation between the patients groups carrying either of the two most frequent mutations, c.1714G>C and c.527A>T (table 2). As with a previous report,[13] homozygous c.1714G>C mutations resulted in earlier symptom onset (23.9±7.1 years, $p<0.01$) and the majority of full-time wheelchair users were in this group. On the other hand, c.1714G>C/c.527A>T compound heterozygous patients first developed symptoms at a later age (37.6±12.6 years, $p<0.01$), and there were no wheelchair-bound patients at the time of genetic analysis in this group. Only three homozygous c.527A>T mutation patients were identified, and their average onset age (32.3±5.7 years) was also higher among total patients (28.4±10.2 years). All three patients were ambulant until the last follow-up visits (29, 40 and 44 years).

Among 212 cases, 80 patients underwent muscle biopsies. Overall pathological findings in our series were compatible with GNE myopathy. The characteristic rimmed vacuoles were observed in the majority (76/80, 95.0%) of the cases. Through the analysis of muscle biopsies from age-matched and biopsy site-matched samples, we found that the histopathological phenotypes were in line with these genotype–phenotype correlations (figure 2). Homozygous c.1714G>C mutations have led to much more advanced pathological changes with severe myofibre atrophy and increased numbers of rimmed vacuoles. Marked adipose tissue replacement was appreciated in a case with reflecting very advanced stage of muscle degeneration.

DISCUSSION

As shown in figure 1, mutations were located throughout the whole open reading frame of the *GNE* gene. The majority (94.8%, 402/424 alleles) of the mutations in our series were missense mutations (table 1), and there were no homozygous null mutations. These results are in accordance with previous reports[7 9] signifying that total loss of GNE function might be

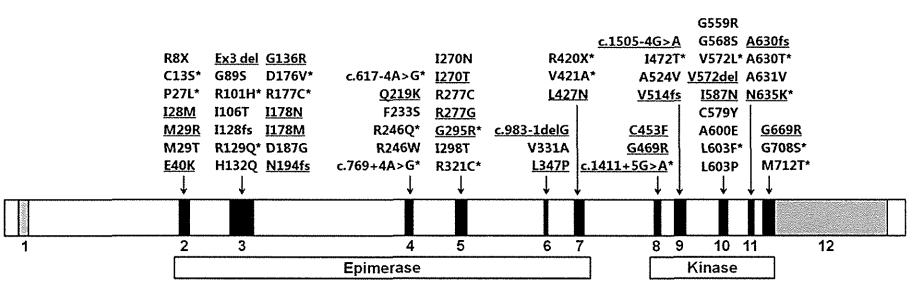

Figure 1 Mutation spectrum of *GNE* in the Japanese population. The mutations are located throughout the whole open reading frame. Twenty-five novel mutations are underlined, and 21 shared mutations are indicated with asterisks.

Table 2 Comparison of clinical course between two most frequent GNE mutations in Japanese population

Mutations	Age at exam (years)		Age at onset (years)		Age at WB (years)		Ambulant
c.1714G>C/c.1714G>C	38.6±13.4	(n=71)	23.9±7.1	(n=65)**	35.4±10.6	(n=28)	n=22
c.1714G>C/other	32.3±13.2	(n=25)	21.9±6.8	(n=22)*	37.0±8.6	(n=4)	n=16
c.1714G>C/c.527A>T	48.9±14.1	(n=38)	37.6±12.6	(n=35)**		(n=0)	n=29
c.527A>T/c.527A>T	37.7±7.7	(n=3)	32.3±5.7	(n=3)		(n=0)	n=3
c.527A>T/other	41.3±11.1	(n=51)	30.6±8.0	(n=46)		(n=2)	n=33
other/other	49.8±14.7	(n=24)	28.8±9.5	(n=24)		(n=2)	n=16
Total	41.6±14.1	(n=212)	28.4±10.2	(n=195)	36.8±11.3	(n=36)	n=118

Dunnett's multiple comparison test (control: total patients) *p<0.05, **p<0.01.
Other: a mutation other than c.1714G>C and c.527A>T; WB, wheelchair-bound.

lethal in human beings. The embryonic lethality of null mutation in *GNE* had also been proved in the mouse model.[14] Only three of total 212 patients carried a nonsense mutation; clinical data were available for two of them. Interestingly, one patient with compound heterozygous c.22C>T (p.Arg8X)/c.1714G>C (p.Val572Leu) mutations developed his first symptoms at the age of 15, while the other patient with c.1258C>T (p.Arg420X)/c.527A>T (p.Asp176Val) mutations developed her symptoms much later, at the age of 45. The similar difference was also observed in the phenotypes of patients with frame-shift mutations. A patient carrying c.383insT (p.I128fs) and c.1714G>C (p.Val572Leu) mutations developed his first symptom at the age of 13, whereas another two patients with c.1541-4del4 (p.Val514fs)/c.527A>T (p.Asp176Val) and c.581delA (p.N194fs)/c.527A>T (p.Asp176Val) mutations had later symptom onset, at the age of 30 and 32 years, respectively. This clinical variation can be explained as it reflects alternative missense mutations, because the two patients with very early onset shared the same missense mutation c.1714G>C, while the patients with the milder phenotype shared c.527A>T.

Among five intronic mutations identified in our series, c.617 −4A>G and c.769 + 4A>G were previously reported as pathological mutations.[7 15] Three novel variants were located at splice junction of exon 6 (c.983–1delG), exon 8 (c.1411 +5G>A) and exon 9 (c.1505–4G>A), raising the high possibility of relevant exons skipping. These variants were not detected in 200 alleles from normal Japanese individuals and also in the single nucleotide polymorphism (SNP) database.

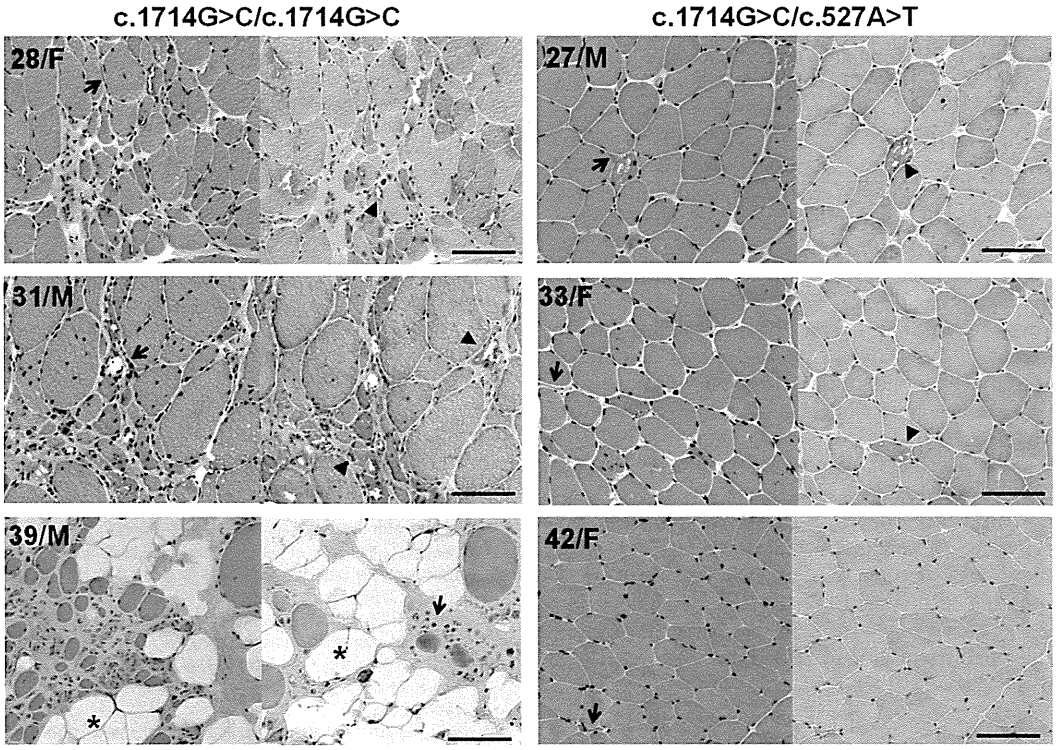

Figure 2 Comparison of muscle pathology between patients with homozygous c.1714G>C (p.Val572Leu) and with compound heterozygous c.1714G>C (p.Val572Leu)/c.527A>T (p.Asp176Val) mutations. Homozygous c.1714G>C (p.Val572Leu) mutations have led to much more advanced histopathological changes compared with compound heterozygous c.1714G>C (p.Val572Leu)/c.527A>T (p.Asp176Val) mutations. Haematoxylin-eosin (left) and modified Gomori trichrome (right) stains of muscle sections from age (c.1714G>C/c.1714G>C: 28, 31 and 39 years, c.1714G>C/c.527A>T: 27, 33 and 42 years) and biopsy site (biceps brachii muscles) matched samples. Bar=100μm; triangles: rimmed vacuoles; arrows: atrophic fibres; asterisks: adipose tissue.

As there are ethnic differences in *GNE* mutation frequencies,[9 16–19] establishing the mutation spectrum and defining predominant mutations in a certain population may be helpful for the diagnosis. Three most common mutations in the Japanese population and their allele frequencies (table 1) were in agreement with previous data.[7 13] The allele frequencies of top two mutations (c.1714G>C and c.527A>T) comprise more than two-third of the total number of alleles suggesting that founder effects are involved in the relatively higher incidence of GNE myopathy in Japan.

Although most of patients showed characteristic pathological features, the existence of exceptional cases with atypical biopsy findings implies that GNE myopathy cannot be totally excluded from the absence of rimmed vacuoles in muscle biopsies. On the other hand, we found 94 patients who were pathologically or clinically suspected but not had mutations in *GNE*. Several cases of VCP myopathy mutations in (*VCP*), myofibrillar myopathy mutations in (*DES*) and reducing body myopathy (*FHL1*) were later identified in this group, suggesting these diseases should be included as differential diagnosis of GNE myopathy.[20]

In terms of genotype–phenotype correlations, we confirmed that homozygosity for c.1714G>C (p.Val572Leu) mutation resulted in more severe phenotypes in clinical and histopathological aspects. In contrast, the second most common mutation, c.527A>T (p.Asp176Val), seems to be a mild mutation as the onset of the disease is much later in the compound heterozygotes with this mutation and c.1714G>C. Several evidences further strengthened the link between the more severe phenotype and c.1714G>C, and between the milder phenotype and c.527A>T. Compound heterozygosity for c.1714G>C and non-c.527A>T mutations resulted in earlier symptom onset (22.9 ± 6.8 years, $p<0.05$) compared with the average onset age of the total group, whereas c.527A>T, both presented as homozygous and as compound heterozygous mutations, lead to slower disease progression (table 2). In addition, only three patients carrying this second most common mutation c.527A>T in homozygous mode were identified, which is much fewer than the number expected from high allele frequency (22.4%), raising a possibility that considerable number of c.527A>T homozygotes may not even develop a disease. In fact, we ever identified an asymptomatic c.527A>T homozygote at age 60 years.[7] Now he is at age 71 years and still healthy. Overall, these results indicate that different mutations lead to different spectra of severity. However, this is a result of a statistical summary that cannot predict clinical course of each individual patient.

Here, we presented the molecular bases of 212 Japanese GNE myopathy patients with 25 novel *GNE* mutations. Based on the current status of knowledge, sialic acid supplementation may lead to considerable changes in the natural course of GNE myopathy within near future. The ongoing identification of *GNE* mutations and further studies regarding the clinicopathological features of each mutation will provide better understanding of GNE myopathy and lead to accelerated development of treatment for this disease.

Acknowledgements The authors thank Kanako Goto and Yuriko Kure for their invaluable technical support and assistant in genetic analysis.

Contributors AC had full access to all of the data in the study and wrote the manuscript; YKH supervised all aspects of this study including study design, data interpretation and manuscript preparation; KM and YO participated in collecting and analysing all the clinical and genetic data; SN, I Nonaka and I Nishino were involved in data analysis and interpretation and also supervised manuscript preparation.

Funding This study was supported partly by Intramural Research Grant 23-4, 23-5, 22-5 for Neurological and Psychiatric Disorders of NCNP; partly by Research on Intractable Diseases, Comprehensive Research on Disability Health and Welfare, and Applying Health Technology from the Ministry of Health Labour and Welfare; and partly by JSPS KAKENHI Grant Number of 23390236.

Competing interests None.

Ethics approval This study was approved by the ethics committee of National Center of Neurology and Psychiatry.

Provenance and peer review Not commissioned; externally peer reviewed.

REFERENCES

1 Nonaka I, Sunohara N, Ishiura S, *et al*. Familial distal myopathy with rimmed vacuole and lamellar (myeloid) body formation. *J Neurol Sci* 1981;51:141–55.
2 Argov Z, Yarom R. "Rimmed vacuole myopathy" sparing the quadriceps. A unique disorder in Iranian Jews. *J Neurol Sci* 1984;64:33–43.
3 Askanas V, Engel WK. New advances in the understanding of sporadic inclusion-body myositis and hereditary inclusion-body myopathies. *Curr Opin Rheumatol* 1995;7:486–96.
4 Nonaka I, Noguchi S, Nishino I. Distal myopathy with rimmed vacuoles and hereditary inclusion body myopathy. *Curr Neurol Neurosci Rep* 2005;5:61–5.
5 Nishino I, Malicdan MC, Murayama K, *et al*. Molecular pathomechanism of distal myopathy with rimmed vacuoles. *Acta Myol* 2005;24:80–3.
6 Eisenberg I, Avidan N, Potikha T, *et al*. The UDP-N-acetylglucosamine 2-epimerase/N-acetylmannosamine kinase gene is mutated in recessive hereditary inclusion body myopathy. *Nat Genet* 2001;29:83–7.
7 Nishino I, Noguchi S, Murayama K, *et al*. Distal myopathy with rimmed vacuoles is allelic to hereditary inclusion body myopathy. *Neurology* 2002;59:1689–93.
8 Keppler OT, Hinderlich S, Langner J, *et al*. UDP-GlcNAc 2-epimerase: a regulator of cell surface sialylation. *Science* 1999;284:1372–6.
9 Eisenberg I, Grabov-Nardini G, Hochner H, *et al*. Mutations spectrum of *GNE* in hereditary inclusion body myopathy sparing the quadriceps. *Hum Mutat* 2003;21:99.
10 Noguchi S, Keira Y, Murayama K, *et al*. Reduction of UDP-N-acetylglucosamine 2-epimerase/N-acetylmannosamine kinase activity and sialylation in distal myopathy with rimmed vacuoles. *J Biol Chem* 2004;279:11402–7.
11 Malicdan MC, Noguchi S, Nonaka I, *et al*. A Gne knockout mouse expressing human *GNE* D176V mutation develops features similar to distal myopathy with rimmed vacuoles or hereditary inclusion body myopathy. *Hum Mol Genet* 2007;16:2669–82.
12 Malicdan MC, Noguchi S, Hayashi YK, *et al*. Prophylactic treatment with sialic acid metabolites precludes the development of the myopathic phenotype in the DMRV-hIBM mouse model. *Nat Med* 2009;15:690–5.
13 Mori-Yoshimura M, Monma K, Suzuki N, *et al*. Heterozygous UDP-GlcNAc 2-epimerase and N-acetylmannosamine kinase domain mutations in the *GNE* gene result in a less severe GNE myopathy phenotype compared to homozygous N-acetylmannosamine kinase domain mutations. *J Neurol Sci* 2012;318:100–5.
14 Schwarzkopf M, Knobeloch KP, Rohde E, *et al*. Sialylation is essential for early development in mice. *Proc Natl Acad Sci USA* 2002;99:5267–70.
15 Ikeda-Sakai Y, Manabe Y, Fujii D, *et al*. Novel Mutations of the *GNE* gene in distal myopathy with rimmed vacuoles presenting with very slow progression. *Case Rep Neurol* 2012;4:120–5.
16 Li H, Chen Q, Liu F, *et al*. Clinical and molecular genetic analysis in Chinese patients with distal myopathy with rimmed vacuoles. *J Hum Genet* 2011;56:335–8.
17 Liewluck T, Pho-Iam T, Limwongse C, *et al*. Mutation analysis of the *GNE* gene in distal myopathy with rimmed vacuoles (DMRV) patients in Thailand. *Muscle Nerve* 2006;34:775–8.
18 Kim BJ, Ki CS, Kim JW, *et al*. Mutation analysis of the *GNE* gene in Korean patients with distal myopathy with rimmed vacuoles. *J Hum Genet* 2006;51:137–40.
19 Broccolini A, Ricci E, Cassandrini D, *et al*. Novel *GNE* mutations in Italian families with autosomal recessive hereditary inclusion-body myopathy. *Hum Mutat* 2004;23:632.
20 Shi Z, Hayashi YK, Mitsuhashi S, *et al*. Characterization of the Asian myopathy patients with VCP mutations. *Eur J Neurol* 2012;19:501–9.

Please cite this article in press as: Gupta et al., Identification of *KLHL41* Mutations Implicates BTB-Kelch-Mediated Ubiquitination as an Alternate Pathway to..., The American Journal of Human Genetics (2013), http://dx.doi.org/10.1016/j.ajhg.2013.10.020

REPORT

Identification of *KLHL41* Mutations Implicates BTB-Kelch-Mediated Ubiquitination as an Alternate Pathway to Myofibrillar Disruption in Nemaline Myopathy

Vandana A. Gupta,[1] Gianina Ravenscroft,[2] Ranad Shaheen,[3] Emily J. Todd,[2] Lindsay C. Swanson,[1] Masaaki Shiina,[4] Kazuhiro Ogata,[4] Cynthia Hsu,[1] Nigel F. Clarke,[5] Basil T. Darras,[6] Michelle A. Farrar,[7] Amal Hashem,[3] Nicholas D. Manton,[8] Francesco Muntoni,[9] Kathryn N. North,[10] Sarah A. Sandaradura,[5] Ichizo Nishino,[11] Yukiko K. Hayashi,[11] Caroline A. Sewry,[9] Elizabeth M. Thompson,[12,13] Kyle S. Yau,[2] Catherine A. Brownstein,[1] Timothy W. Yu,[1] Richard J.N. Allcock,[14] Mark R. Davis,[15] Carina Wallgren-Pettersson,[16] Naomichi Matsumoto,[17] Fowzan S. Alkuraya,[3] Nigel G. Laing,[2] and Alan H. Beggs[1,*]

Nemaline myopathy (NM) is a rare congenital muscle disorder primarily affecting skeletal muscles that results in neonatal death in severe cases as a result of associated respiratory insufficiency. NM is thought to be a disease of sarcomeric thin filaments as six of eight known genes whose mutation can cause NM encode components of that structure, however, recent discoveries of mutations in non-thin filament genes has called this model in question. We performed whole-exome sequencing and have identified recessive small deletions and missense changes in the Kelch-like family member 41 gene (*KLHL41*) in four individuals from unrelated NM families. Sanger sequencing of 116 unrelated individuals with NM identified compound heterozygous changes in *KLHL41* in a fifth family. Mutations in *KLHL41* showed a clear phenotype-genotype correlation: Frameshift mutations resulted in severe phenotypes with neonatal death, whereas missense changes resulted in impaired motor function with survival into late childhood and/or early adulthood. Functional studies in zebrafish showed that loss of Klhl41 results in highly diminished motor function and myofibrillar disorganization, with nemaline body formation, the pathological hallmark of NM. These studies expand the genetic heterogeneity of NM and implicate a critical role of BTB-Kelch family members in maintenance of sarcomeric integrity in NM.

Nemaline myopathy (NM) is a rare congenital disorder primarily affecting skeletal muscle function. Clinically, NM is a heterogeneous group of myopathies of variable severity.[1,2] The "severe" congenital form of NM presents with reduced or absent spontaneous movements in utero leading to severe contractures or fractures at birth and respiratory insufficiency leading to early mortality. Individuals with the "intermediate" congenital form of NM have antigravity movement and independent respiration at delivery but exhibit delayed motor milestones and require ventilatory support later in life. The "typical" congenital form of NM usually presents in the neonatal period or first year of life with hypotonia, weakness, and feeding difficulties with less prominent respiratory involvement. In these cases, the disease is usually static or very slowly progressive, and many individuals remain ambulant for much of their lives.[3] The defining diagnostic feature of all forms of NM, irrespective of genetic mutation, is the presence of numerous red-staining rods with Gomori trichrome stain that appear as rod-shaped electron-dense structures termed "nemaline bodies" by electron microscopy.[4] These nemaline bodies are most frequently cytoplasmic; however, the presence of intranuclear rods has also been reported.[5]

NM is a genetically heterogeneous condition, and mutations in eight different genes have been identified that are associated with dominant and/or recessive forms of this disease.[6–13] Mutations in these genes cause about 75%–80% of NM cases, suggesting the involvement of additional unidentified genes in disease etiology.

[1]Division of Genetics and Genomics, The Manton Center for Orphan Disease Research, Boston Children's Hospital, Harvard Medical School, Boston, MA 02115, USA; [2]Western Australian Institute for Medical Research and the Centre for Medical Research, University of Western Australia, Nedlands, Western Australia 6009, Australia; [3]Developmental Genetics Unit, King Faisal Specialist Hospital and Research Center, Riyadh 11211, Saudi Arabia; [4]Department of Biochemistry, Yokohama City University, Graduate School of Medicine, 3-9 Fukuura, Kanazawa-ku, Yokohama 236-0004, Japan; [5]Institute for Neuroscience and Muscle Research, Children's Hospital at Westmead and Discipline of Paediatrics and Child Health, University of Sydney, Sydney 2145, Australia; [6]Department of Neurology, Boston Children's Hospital, Harvard Medical School, Boston, MA 02115, USA; [7]Department of Neurology, Sydney Children's Hospital, Randwick NSW 2032, Australia; [8]Department of Surgical Pathology, SA Pathology at the Women's and Children's Hospital, North Adelaide, South Australia 5006; [9]Dubowitz Neuromuscular Centre, Institute of Child Health and Great Ormond Street Hospital, London WC1N 1EH, UK; [10]Murdoch Childrens Research Institute, The Royal Children's Hospital, Parkville, Victoria 3052, Australia; [11]Department of Neuromuscular Research, National Institute of Neuroscience, National Center of Neurology and Psychiatry, Tokyo 187-8502, Japan; [12]Department of Paediatrics, University of Adelaide, Adelaide, South Australia 5000, Australia; [13]SA Clinical Genetics Service, SA Pathology at the Women's and Children's Hospital, North Adelaide, South Australia 5006, Australia; [14]Lotterywest State Biomedical Facility Genomics and School of Pathology and Laboratory Medicine, University of Western Australia, Perth, Western Australia 6000, Australia; [15]Department of Anatomical Pathology, Royal Perth Hospital, Perth, Western Australia 6000, Australia; [16]The Folkhälsan Institute of Genetics, Samfundet Folkhälsan, Biomedicum Helsinki, PB 63 (Haartmaninkatu 8), and Department of Medical Genetics, Haartman Institute, University of Helsinki, Helsinki 00014, Finland; [17]Department of Human Genetics, Yokohama City University, Graduate School of Medicine, 3-9 Fukuura, Kanazawa-ku, Yokohama 236-0004, Japan
*Correspondence: beggs@enders.tch.harvard.edu
http://dx.doi.org/10.1016/j.ajhg.2013.10.020.

Therefore, we performed whole-exome sequencing (WES) combined, when applicable, with autozygome analysis to identify mutations in novel genes that underlie the disease pathology in a cohort of individuals affected with NM with unknown genetic diagnosis. All subjects were enrolled following informed consent and research was conducted according to the protocols approved by the Institutional Review Boards of the respective institutions in which these individuals were recruited. Molecular screening was performed on genomic DNA isolated from blood samples following standard protocols.

We performed whole-exome or whole-genome sequencing on a cohort of 60 unrelated NM probands through Boston Children's Hospital Gene Partnership facility. Molecular screening was performed on genomic DNA isolated from blood samples with standard protocols. Whole-blood DNA was subjected to solution capture (SureSelect Human All Exon V4, Agilent Technologies) to generate barcoded whole-exome sequencing libraries. Libraries were sequenced on an Illumina HiSeq 2000, employing paired end reads (100 bp × 2) to a mean target coverage of 96.5% and a mean read depth of 71.6. Alignment, variant calling, and annotation were performed with a custom informatics pipeline employing BWA,[14] Picard, and ANNOVAR[15] focusing on rare (<3% in db SNP135, 1000 Genomes Project Database, and the [EVS] National Heart, Lung, and Blood Institute Exome Sequencing Project Exome Variant Server) protein affecting changes in known and novel human disease genes. Alternatively, probands for families 203 and 832 were sequenced to greater than 50× depth by Axeq Technologies on an Illumina HiSeq 2000 following Agilent SureSelect Exome enrichment with their standard Exome Sequencing service. Whole-exome sequencing identified homozygous mutations of *KLHL41* in two unrelated families, suggesting this gene to be a candidate for NM. All *KLHL41* mutations are numbered relative to the mRNA sequence NM_006063.2 (where position 1 is the first base of the initiating MET codon) and protein NP_006054.2. Family 1 is a nonconsanguineous family of Vietnamese origin. Proband 203-1 is a 16-year-old female with an intermediate form of NM with a high-arched palate, dysarthria, and scoliosis who has required ventilatory support since childhood. WES identified an apparently homozygous c.103T>C transition in exon 1 resulting in a p.Cys35Arg substitution in this individual (Figure 1A). This variant was present as heterozygous in the father and absent in the mother. Copy number analysis in the affected region showed a heterozygous deletion in the mother and the proband, c.(?_-77)_(*602_?)del. Therefore, individual 203-1 is compound heterozygous for a deletion involving a portion of *KLHL41* and a KLHL41 p.Cys35Arg missense change. The second proband (832-1), who is adopted of Russian origin, is ambulant at age 12 and exhibits the typical congenital form of NM. WES identified a homozygous deletion of one base and an insertion of four bases c.459delinsACTC in the proband resulting in a single amino acid insertion, p.Ser153_Ala154insLeu in the protein (Figure 1A).

Whole-exome sequencing in probands with severe NM in Australian and Saudi Arabian cohorts resulted in identification of *KLHL41* mutations in two further families. The first (6462) is a consanguineous family of Persian origin from Afghanistan with one child (D12-203) affected with severe NM and four unaffected children (see Figure S1 available online). Homozygosity mapping was performed on the proband with the Illumina HumanCytoSNP-12 array, and the only known NM loci found within homozygous regions were *CFL2* (MIM 601443) and *NEB* (MIM 161650); however, both were excluded following Sanger sequencing, as was *ACTA1* (MIM 102610), which is the most common cause of simplex NM cases. WES of DNA from proband D12-203 was performed at the Lotterywest Sate Biomedical Facility Genomics Node, Royal Perth Hospital, Western Australia.[13] WES identified 453 heterozygous or homozygous variants. Application of the homozygosity data to the list of candidates reduced this to seven candidate variants. Two of these seven candidate variants were in skeletal-muscle-specific genes and of these the most likely candidate was a homozygous deletion within *KLHL41* (chr2: 170382132–170382139; c.1748_1755delAAGGAAAT, p.Lys583Thrfs*7) (Figure 1A). The deletion was confirmed by Sanger sequencing. Both parents and two unaffected siblings were heterozygous for the deletion, and two further unaffected siblings were homozygous for the normal allele.

Family 12DG1177, from a Saudi Arabian cohort is consanguineous (Figure S1). The male proband (12DG1177-1) was a newborn with severe hypotonia, dislocation of hips and knees, and facial dysmorphism in the form of micrognathia and cleft palate. There was a positive family history of two previous sibs who died of unknown causes soon after birth, as well as three healthy living sibs. The proband died of cardiorespiratory arrest shortly after intubation at less than 24 hr of age. Exome capture was performed with TruSeq Exome Enrichment kit (Illumina) as described earlier.[16] Only novel coding and splicing homozygous variants within the autozygome of the affected individual were considered. After filtering, 8,653 homozygous, coding, or splice variants were present, and autozygosity mapping, dbSNP, and analysis of 240 control Saudi exomes finally led to the identification of 18 candidate variants. The only truncating change was a single base deletion in *KLHL41* (c.641delA). This deletion was present in the coding region of exon 1 of *KLHL41* resulting in the frameshift change p.Asn214Thrfs*14 (Figure 1A).

Subsequent screening for *KLHL41* mutations in 116 individuals affected with severe, intermediate, or typical congenital forms of NM in the Boston and Australian NM Cohorts by Sanger sequencing identified a further family (D10-236) with compound heterozygous mutation (c.581_583delAAG, p.Glu194del and c.1238C>T, p.Ser413Leu) in proband. This individual is of Chinese

Please cite this article in press as: Gupta et al., Identification of *KLHL41* Mutations Implicates BTB-Kelch-Mediated Ubiquitination as an Alternate Pathway to..., The American Journal of Human Genetics (2013), http://dx.doi.org/10.1016/j.ajhg.2013.10.020

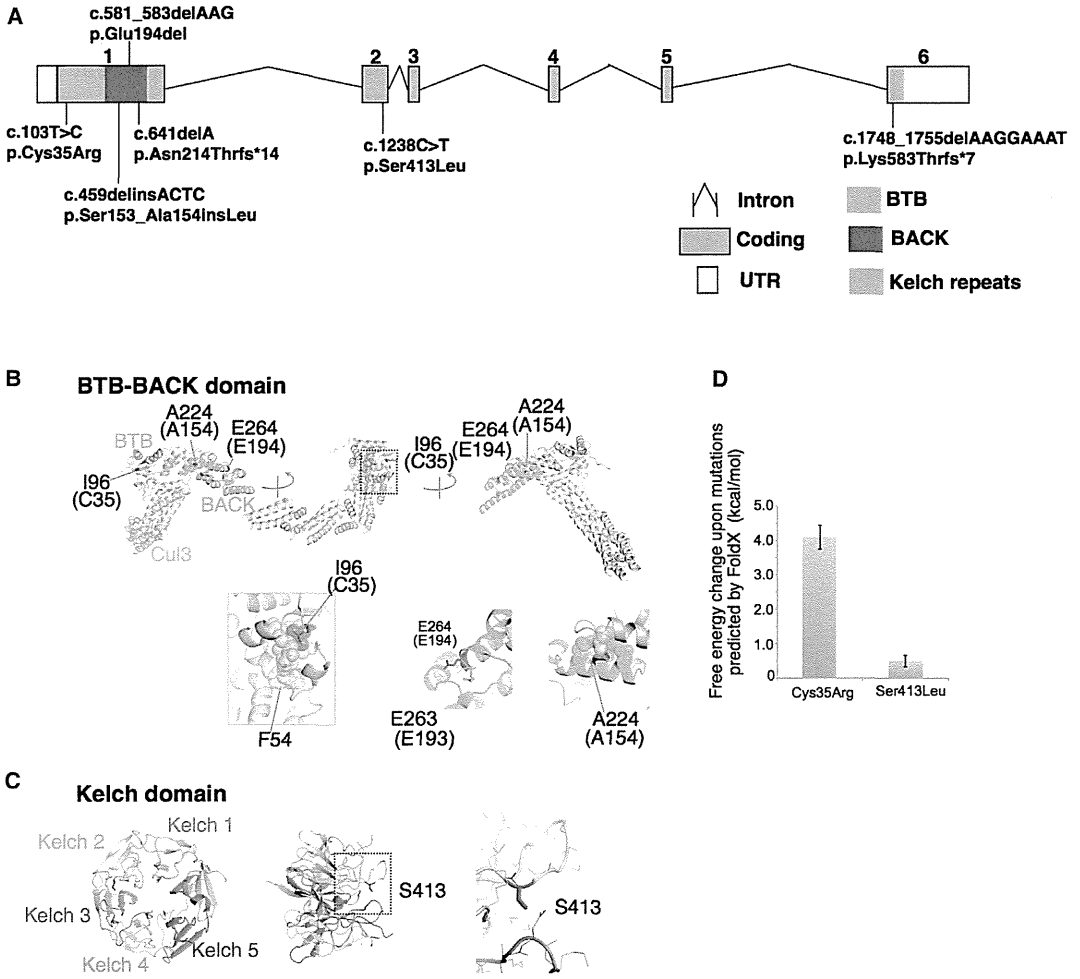

Figure 1. Overview of Mutations in *KLHL41* and Their Effect on Protein Structure

(A) Schematic representation of mutations in *KLHL41*. Boxes represent exons 1–6. Conserved domains of KLHL41 are indicated as follows: BTB (blue), BACK (red), and Kelch repeats (green). The BTB and BACK domains are encoded by exon 1 and the five Kelch repeats are encoded by exons 1–6.

(B and C) Crystal structures of the BTB-BACK domain of human Kelch-like protein (KLHL11) in complex with CUL3 (Protein Data Bank code 4AP2) (B) and the Kelch domain of rat KLHL41 (PDB code 2WOZ) (C). α helices, β strands, and loops are drawn as ribbons, arrows, and threads, respectively. The squared areas correspond to the close-up views in the insets. In (B), the BTB and BACK domains are colored pink and green, respectively, whereas CUL3 is colored yellow, except that Ile96, Ala224, and Glu264 (Cys35, Ala154, and Glu194 in human KLHL41, respectively) are colored red. The side chains of these residues and Glu263 (Glu193 in human KLHL41) are shown as sticks with the indications of amino acid numbers for human KLHL11 and those for human KLHL41 in parentheses. Side chains involved in hydrophobic cores around Ile96 and Ala224 are drawn in van der Waal's representation. In (C), the Kelch domain is color-coded to indicate each Kelch repeat, except that Ser413 is colored red. The side chain of Ser413 is shown as sticks. Molecular structures are drawn with PyMOL.

(D) Predicted free energy changes upon the substitutions of KLHL41 with FoldX software.

origin and exhibited the typical congenital form of NM. The detailed clinical features of affected individuals with mutations identified in *KLHL41* are presented in Table 1.

Overall, WES and Sanger sequencing resulted in identification of seven different mutations in Kelch-like family member 41 (*KLHL41*), previously known as *KBTBD10*, sarcosin, or *KRP1*, in affected NM individuals from five unrelated families (Figure 1A). Muscle histology was typical for NM: biopsies from probands of three different families (D12-203, 832-1, and 10-236) exhibited abnormal Gomori trichrome staining with presence of sarcoplasmic rods that varied from numerous small rods to fewer large rods in multiple myofibers (Figure 2A). No intranuclear rods or cores were seen. The missense changes identified in *KLHL41* are predicted to be pathogenic by polyphen, SIFT and pMUT and the mutated amino-acid residues are conserved in all representative species during evolution (Figure S2). The neighboring areas surrounding the sites of insertion or deletion are also relatively conserved, suggesting a structural or functional requirement for the altered amino acid residues (Figure S2). Sequencing of family members revealed that *KLHL41*

Table1. Clinical Manifestations in Affected Individuals Harboring *KLHL41* Mutations

Proband ID	cDNA Change	Amino Acid Change	Clinical Category	Sex	Nationality	Pregnancy and Delivery	Alive at Age/Mobility/ Age at Death	Associated Features
203-1	c.103T>C c.(?_-77)_(*602_?)del	p.Cys35Arg Heterozygous p.0? Heterozygous	Intermediate	F	Vietnamese	Normal	16 yrs, uses wheelchair (ambulant 24–36 mo)	Ventilated 24 hr from 5 yrs. High-arched palate, dysarthria Scoliosis
832-1	c.459delinsACTC	p.Ser153_Ala154insLeu Homozygous	Other forms (grade of severity: mild)	M	Russian	No data	12 yrs, ambulant	Distal weakness > proximal distal contractures
D10-236	c.581_583delAAG c.1238C>T	p.Glu194del Heterozygous p.Ser413Leu Heterozygous	Typical form	M	Chinese	Normal - h 40	5 yrs, ambulant	VSD, finger contractures, focal renal echogenicity
D12-203	c.1748_1755del AAGGAAAT,	p.Lys583Thrfs*7 Homozygous	Fetal akinesia sequence	M	Persian	Polyhydramnios, breech presentation, emergency Cesarean section - h 31+2	Died at 3 mo (active support discontinued)	Arthrogryposis, macrocephaly, hypospadias No antigravity movements at birth
12DG1177	c.641delA	p.Asn214Thrfs*14 Homozygous	Severe form Fetal akinesia sequence	M	Saudi Arabian	Fetal movements weak, breech presentation	Died during 1st day of life	Dislocation of hips and knees, cleft palate, micrognathia, narrow chest

mutations showed a segregation pattern compatible with a recessive mode of inheritance in all families (Figure S1). Severe phenotypes associated with genetic null mutations and intermediate or typical congenital forms with mutations that should results in presence of residual protein, suggests a phenotype-genotype correlation in individuals affected with *KLHL41* mutations.

KLHL41 belongs to the family of BTB-Kelch domain-containing proteins.[17–20] Mutations in two other members of this family, *KBTBD13* (MIM 613727), and most recently *KLHL40* (MIM 615430), have been associated with a clinically distinct form of congenital myopathy exhibiting nemaline bodies, as well as multiminicores and severe NM, respectively.[12,13] To evaluate the impacts of the *KLHL41* mutations on the protein structure, we mapped them onto the crystal structures of the BTB-BACK domain of human KLHL11 in complex with human CUL3, a subunit of E3 ubiquitin ligases, (PDB code 4AP2)[21] and the Kelch domain of rat KLHL41 (PDB code 2WOZ),[22] analogous to those domains of human KLHL41. The Cys35 side chain is involved in a hydrophobic core of the BTB domain, which makes van der Waals contacts with Phe54 of Cul3 (Figure 1B). The p.Cys35Arg substitution present in affected individual 203-1 would likely destabilize the hydrophobic core and thereby impair the interaction with Cul3. This was supported by the FoldX result, in which free energy change upon the p.Cys35Arg substitution was predicted to be over 4 kcal/mol, which can be interpreted as considerable destabilization of a protein structure (Figure 1D; Figure S3).[23] In proband 832-1, a Leu residue is inserted between the amino acid positions 153 and 154 in the center of a helix, in which several residues are involved in a hydrophobic core of the BACK domain (Figure 1B). This amino acid insertion is likely to destabilize the BACK domain fold. In proband D10-236, the p.Ser413Leu substitution was mapped to a loop region, which is located near the substrate-binding region of the Kelch repeat 2 (Figure 1C; Figure S1B). A FoldX calculation predicted that the p.Ser413Leu substitution would have minimal effect on stability of the Kelch domain (Figure 1D). The effect of Glu194 deletion at the N-terminal end of an α helix can be compensated by the presence of Glu193 located in the loop (Figure 1B). Nonetheless, it cannot be excluded that the p.Ser413Leu and p.Glu194del changes alter the protein solubility or aggregate tendency and/or impair substrate binding. The conserved nature of the mutated KLHL41 domains, as well as the potential role of the mutations in disrupting those structural domains, supports the likely pathogenicity of these mutations.

The localization of KLHL41 in skeletal muscles was investigated by immunofluorescence of mouse FDB cultured myofibers and human skeletal muscle cryosections. Immunofluorescence with two different antibodies against N-terminal (Sigma, AV38732) and C-terminal parts of human KLHL41 (Abcam, ab66605) was performed, and z stacks were acquired by confocal microscopy as described

Please cite this article in press as: Gupta et al., Identification of *KLHL41* Mutations Implicates BTB-Kelch-Mediated Ubiquitination as an Alternate Pathway to..., The American Journal of Human Genetics (2013), http://dx.doi.org/10.1016/j.ajhg.2013.10.020

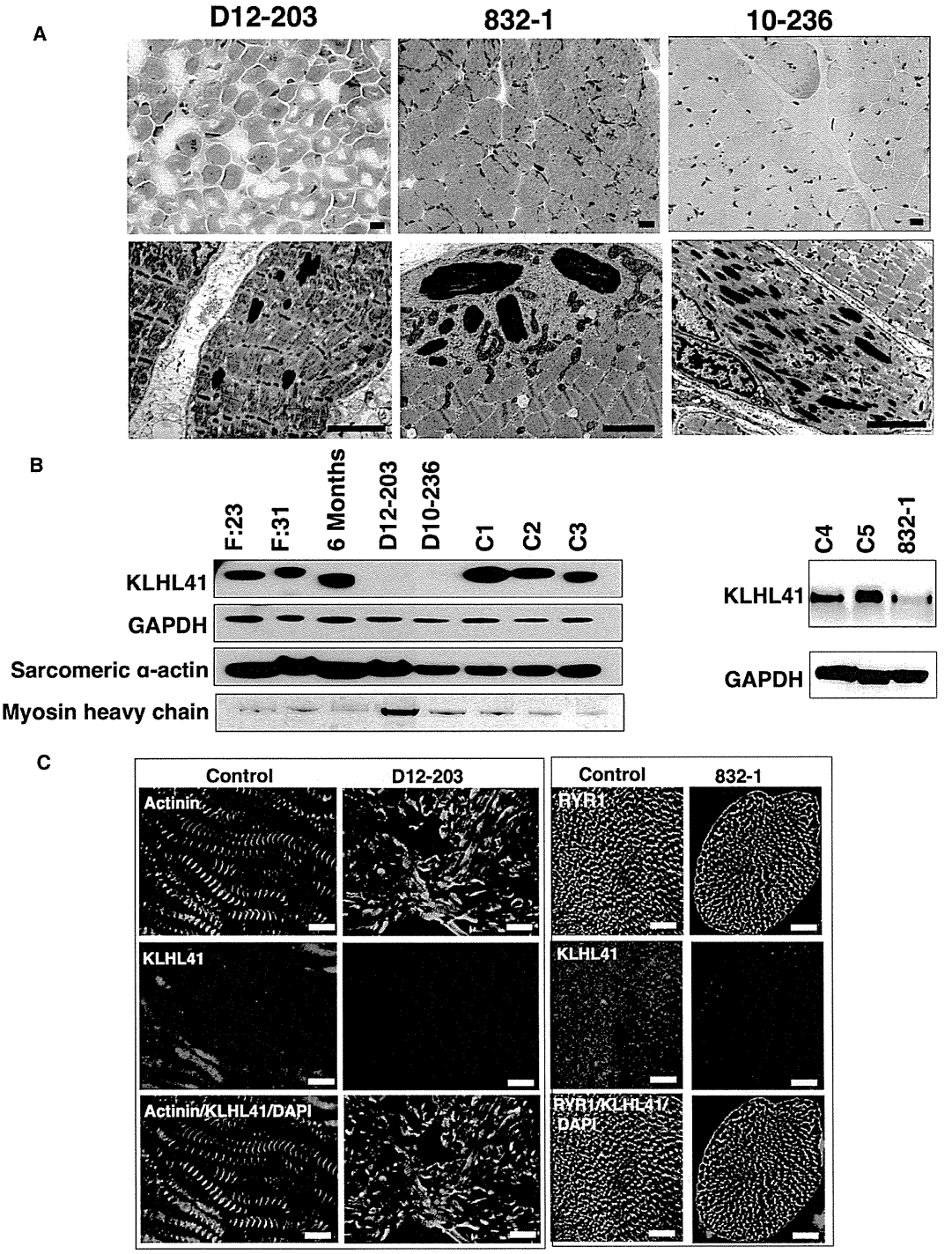

Figure 2. Muscle Pathology and Expression of KLHL41 Levels and Localization in Muscle of Affected Individuals

(A) Light microscopy of Gomori trichrome stained skeletal muscle from affected individuals with *KLHL41* mutations show cytoplasmic nemaline bodies (top panel). Electron microscopy of affected muscles reveals rods of variable frequency and size and severe myofibrillar disarray (bottom panels). (Scale bars represent 2 μm). Affected individuals' IDs are indicated at top.

(B) Immunoblotting analysis of KLHL41 levels in affected and unaffected muscles. A decrease in protein levels was observed in individuals with *KLHL41* mutations in comparison to normal control muscles. Immunoblotting with sarcomeric actin or Coomassie staining of myosin heavy chain showed no abnormal accumulation of sarcomeric proteins in affected muscles. Immunostaining for GAPDH was used for loading controls. Lanes: F:23, 23 week control fetus; F:30, 31 week control fetus; 6-month-old control baby, C1–C5 are normal age-matched control muscles.

(C) Immunofluorescence for KLHL41 in control and affected individual muscle biopsies showed highly reduced levels of KLHL41 in longitudinally oriented (left) or transverse sections (right) of skeletal muscles from affected individuals. Scale bars represent 50 μm.

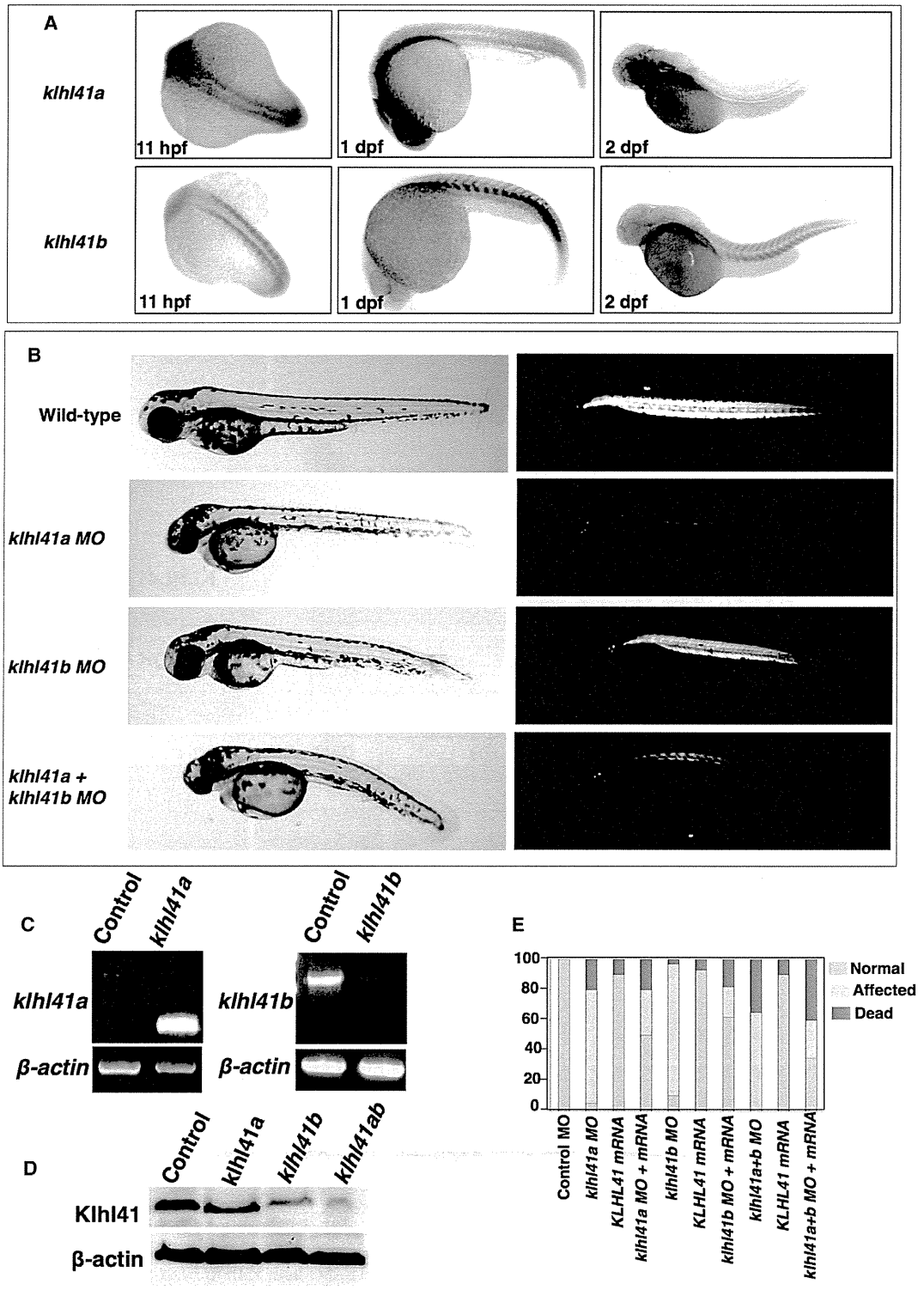

Figure 3. Characterization and Knockdown of Zebrafish Orthologs of *KLHL41*

(A) In situ hybridization of the zebrafish Klhl41 genes shows early expression during myogenesis in developing somites (11 hr after fertilization). *Klhl41a* is expressed in brain, eyes, and muscle at 1 dpf. Later in development expression is largely restricted to brain and heart (2 dpf), although low levels of expression in axial slow skeletal myofibers cannot be excluded due to limited sensitivity of the assay. *Klhl41b* expression is localized to skeletal muscle and heart at all developmental stages (1–2 dpf).

(B) Knockdown of Klhl41 genes in zebrafish using antisense morpholinos results in myopathic changes. Live microscopy of zebrafish embryos at 3 dpf reveals leaner and smaller bodies in comparison to wild-type (WT) fish. Under polarized microscopy, zebrafish embryos

(legend continued on next page)

previously.[24] Immunofluorescence with both antibodies resulted in similar staining patterns; however, due to lower background staining, the C-terminal antibody was used for further studies. Costaining with sarcomeric markers in longitudinal planes showed that KLHL41 staining predominated over the I-bands of the sarcomere and at perinuclear regions in human biopsies (Figure 2C) and murine cultured myofibers (Figure S4). Analysis of transverse sections of myofibers from control human biopsies revealed KLHL41 staining in a ring pattern around the myofibrils, generally colocalizing with ryanodine receptors (RYR1), which are a marker of the sarcoplasmic reticulum (Figure S5). Together, these observations suggest that KLHL41 localizes over (but not within) I bands, likely in association with the terminal cisternae of the sarcomplasmic reticulum (SR) and longitudinal vesicles of the SR present in the I-band area at the triadic regions (Figure S4). Colocalization studies with the ER marker protein disulfide isomerase (PDI) in myofibers and skeletal muscles further confirmed the localization of KLHL41 in SR-ER membranes (Figures S4). This overall localization pattern is most consistent with localization to the endoplasmic reticulum (ER) around myonuclei and to microdomains of the SR with ER characteristics.[25] Previous studies suggested that the closely related NM protein, KLHL40, localized at A-bands,[13] but double label immunofluorescence studies of both longitudinal and transverse sections here reveal that it appears colocalized with RYR1, around but not within the myofibrils in cultured myofibers and human skeletal muscles in a pattern overlapping, but not identical to, that of KLHL41 (Figures S4 and S5). These associations of proteins whose defects cause NM with the ER/SR contrasts with previously known NM proteins, all of which are sarcomeric thin filament components, with the exception of KBTBD13 whose localization is not well known.

In mouse tissues, immunoblotting detected KLHL41 in skeletal muscle and diaphragm (Figure S6). In cultured murine C2C12 cells, KLHL41 levels increased during differentiation to myotubes (Figure S6). Immunoblotting of affected skeletal muscle extracts revealed greatly reduced levels of KLHL41 in individuals with *KLHL41* mutations (Figure 2B) and immunofluorescence microscopy of affected individuals' skeletal muscles also showed that KLHL41 levels were greatly reduced in their myofibers (Figure 2C).

Cell culture studies have shown that KLHL41 interacts with nebulin, N-RAP (Nebulin-related anchoring protein), and actin in skeletal muscle and promotes the assembly of myofibrils.[26] KLHL41 regulates skeletal muscle differentiation as overexpression or knockdown inhibited C2C12 myoblast differentiation.[27] Knockdown of *Klhl41* in cultured cardiomyocytes resulted in sarcomeric disorganization with thickening of Z-lines as seen in NM.[28] However, the exact functions of KLHL41 in disease pathology are unknown. Recent studies have identified mutations in two other closely related family members *KBTBD13* and *KLHL40* as causes of NM suggesting the crucial requirement for several Kelch family proteins in skeletal muscle function.[12,13] To investigate the functional role of KLHL41 in vertebrate skeletal muscle development, we employed zebrafish as a model system. Zebrafish have two duplicated orthologs (*klhl41a* and *klhl41b*) that share ~80% similarity with *KLHL41*. Zebrafish whole-mount in situ hybridization was performed to study the spatio-temporal expression of these genes during zebrafish development as described previously.[29] Specifically, RNA probes specific for each Klhl41 gene were generated by amplification of the 3′ UTRs from a cDNA library of 2 day postfertilization (dpf) zebrafish embryos, followed by in vitro transcription to generate digoxigenin-labeled antisense transcripts (primer sequences are provided in Table S1). Whole-mount in situ hybridization showed ubiquitous expression of *klhl41a* during early development at 1 dpf, but by 2 dpf, *klhl41a* transcripts were virtually undetectable in the major axial skeletal muscles. In contract, *klhl41b* expression was predominantly seen in striated muscles, and strong expression in heart and skeletal muscles was observed throughout zebrafish development to at least 5 dpf (Figure 3A).

The effect of KLHL41 deficiency in zebrafish was studied by knocking down the Klhl41 genes with antisense morpholinos. Two independent morpholinos targeting an exon-intron spice site and translational start site were designed for both genes (morpholino sequences are provided in Table S2). As initial experiments with both morpholinos for each transcript resulted in similar phenotypes, we performed the remainder of our studies with the splice-site morpholinos (7 ng). *klhl41a* morphants exhibited leaner bodies, smaller eyes, and pericardial edema as seen in other myopathy models (n = 65–110) (Figure 3B).[30,31] Examination of 3 dpf morphants with polarized light showed reduced birefringence in axial skeletal muscles suggesting disorganized skeletal muscle structure (Figure 3B; Figure S7). Knockdown of *klhl41b*

exhibit a reduction in birefringence in morphant fish, quantified in ImageJ as described (WT controls: 100% ± 5.9% *klhl41a*: 23% ± 3.0%; *klhl41b*: 31% ± 8.2%; *klhl41ab*: 16% ± 4.2%). Double knockdown fish show a more severe skeletal muscle phenotype than single morphants.

(C) RT-PCR analysis showed knockdown of normal transcripts in the morphant fish.

(D) Immunoblot analysis showed reduction in Klhl41 levels in *klhl41a*, *klhl41b*, and *klhl41ab* fish. Klhl41 antibody recognizes both klhl41a and klhl41b and therefore show immunoreactibility to the other gene in the single morphants that is highly reduced in double morphants.

(E) Overexpression of human *KLHL41* mRNA restores the skeletal muscle phenotypes of *klhl41a/b* single and double morphants suggesting morpholino specificity. The mRNA concentration used to rescue were as follows: *klhl41a* (50 pg), *klhl41b* (75 pg), *klhl41a+b* (60 pg of each)

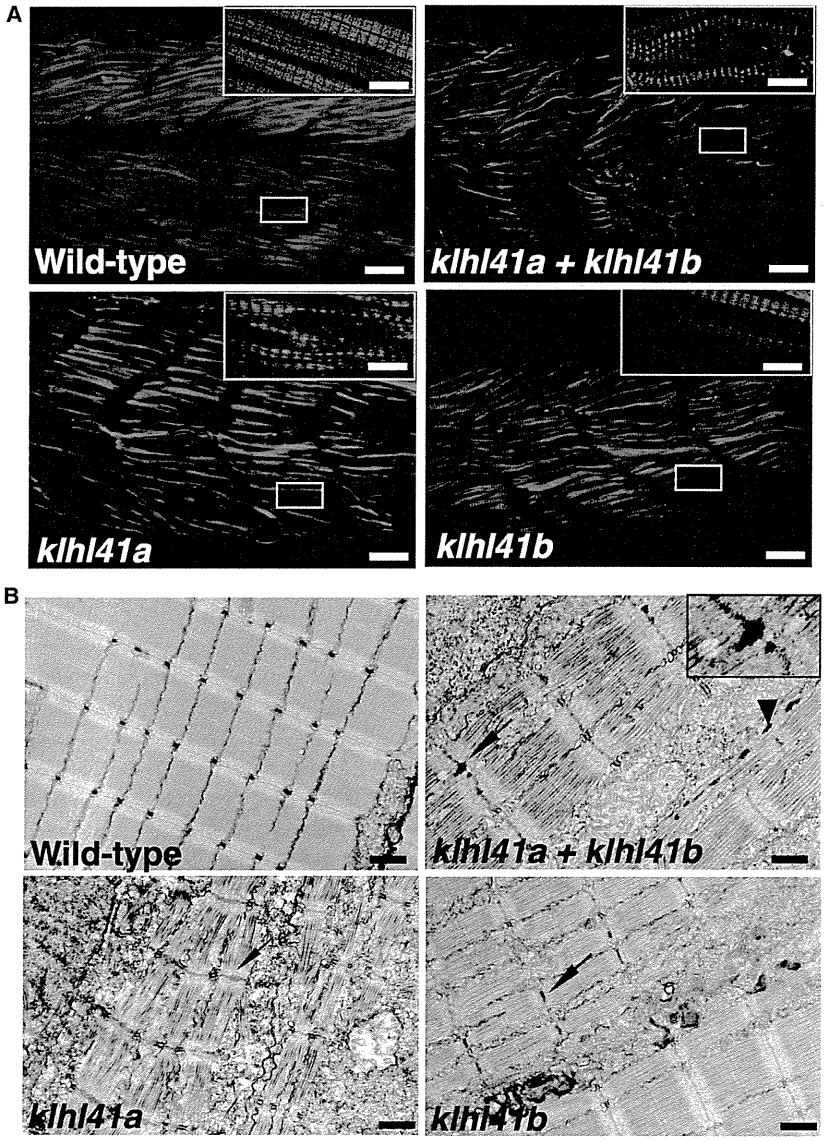

Figure 4. Loss of *klhl41* Function in Zebrafish Recapitulates the Disease Pathology of Human Nemaline Myopathies
(A) Whole-mount staining of 3 dpf zebrafish embryos with phalloidin showed extensive myofibrillar disarray of myofibers in *klhl41* morphant fish (scale bar represents 2 μm). Three dpf embryos fixed in 4% paraformaldehyde were incubated with phalloidin (Invitrogen, A12380, 1:40) overnight at 4°C. Skeletal muscles of klhl41-deficient embryos were smaller and exhibited an overall reduction of myofibrillar organization (inset, high magnification).
(B) Electron microscopy of klhl41-deficient skeletal muscle revealed thickened Z-lines in *klhl41a* or *klhl41b* morphants. In addition, skeletal muscle of double knockdown fish contained electron dense bodies, reminiscent of nascent nemaline rods (arrowhead, nemaline bodies like structures; arrow, thickened Z-lines) (scale bar represents 1 μm).

resulted in reduced birefringence without any other significant abnormalities (n = 82–132). Targeting both *klhl41a* and *klhl41b* (7 ng each) resulted in curved bodies with a 30% reduction in size along with small eyes and pericardial edema (n = 89–103), compared to fish injected with control morpholino (14ng). *klhl41a* morphant fish die by 3 dpf while *klhl41b* morphants typically did not survive past 5 dpf. Knockdown of both genes was lethal by 3 dpf. Double knockdown fish exhibited severely disorganized muscle (measured by reduced birefringence) compared to controls and either of the single knockdowns. RT-PCR and immunoblotting confirmed the knockdown of *klhl41a* and *klhl41b* transcripts and a reduction in protein levels (Figures 3C and 3D). Overexpression of human *KLHL41* mRNA in the double morphants resulted in a significant increase in the number of surviving fish with normal birefringence suggesting the specificity of morpholino injections and demonstrating the ability of this single evolutionary ortholog to complement both zebrafish genes (Figure 3E). Behavioral characterization of 3 dpf morphant fish, knocked down for either or both Klhl41 genes, using the touch-evoked response assay showed significantly diminished motility in comparison to control fish (WT fish: 5.74 ± 0.98 cm/0.1 s; *klhl41a*: 1.32 ± 0.61 cm/0.1 s; *klhl41b*: 2.00 ± 0.49 cm/0.1 s; *klhl41ab*: 0.73 ± 0.39 cm/0.1 s), suggesting a significant degree of overall muscle weakness (Movies S1, S2, S3, and S4).[32] To visualize abnormalities in sarcomeric architecture, whole-mount staining of morphant fish and control zebrafish embryos was performed with phalloidin to stain the actin-thin filaments. Although well-organized myofibrillar striations (i.e., sarcomeres) were observed, the myofibrils in *klhl41* morphants tended to be thinner and were highly disorganized relative to control fish (Figure 4A). The myofibrilar disorganization in *klhl41* morphants was also evident by evaluation of ultrathin toluidine blue sections of control and morphant fish (Figure S7). The main diagnostic feature of NM is the presence of nemaline rods with or without Z-line streaming in skeletal muscle. Ultrastructural examination of zebrafish skeletal muscle by electron microscopy showed Z-line thickening in both *klhl41a* and *klhl41b* morphant fish (Figure 4B). Knockdown of both *klhla* and *klhl41b* resulted in the presence of numerous electron-dense structures, reminiscent of small or nascent nemaline bodies, in addition to Z-line thickening (Figure 4B). Given the differences in temporal expression of *klhl41a* (early embryogenesis) and *klhl41b*

Please cite this article in press as: Gupta et al., Identification of *KLHL41* Mutations Implicates BTB-Kelch-Mediated Ubiquitination as an Alternate Pathway to..., The American Journal of Human Genetics (2013), http://dx.doi.org/10.1016/j.ajhg.2013.10.020

(maintained later in development), and the high degree of structural and functional conservation (both are rescued by the single human transcript), it is likely that increased severity of *klhl41a* morphants is due to this being the predominant embryonic isoform at the early stages targeted by morpholino injections.

Extensive skeletal muscle disorganization associated with sarcomeric abnormalities in morphant fish points toward a function of KLHL41 in skeletal muscle development and maintenance. Mutations affecting the closely related BTB-Kelch family member KLHL40 have recently also been reported to cause nemaline myopathy.[13] While *KLHL40* mutations resulted in a severe clinical presentation in most of the affected individuals, KLHL41 abnormalities are associated with a spectrum of phenotypes from severe with neonatal death, to survival into late childhood. However, no significant differences were seen in skeletal muscle pathology. KLHL40 contains a putative nuclear localization sequence (NLS) and is expressed throughout muscle differentiation, whereas KLHL41 lacks NLS and is expressed in late differentiation (Figure S8).[13] KLHL41 and many other BTB domain-containing Kelch family members are known to interact with Cul3 ubiquitin ligase to form functional ubiquitination complexes with proteins targeted for degradation.[21,33] KLHL41, which has been shown to interact with nebulin,[34] is now the third BTB-Kelch family member to be identified as a cause of NM when mutated. We hypothesize that improper surveillance and degradation of aberrant thin-filament proteins might explain the convergent pathological and clinical phenotypes associated with mutations of thin filament and BTB-Kelch family member genes in NM.

Supplemental Data

Supplemental Data include eight figures, two tables, and four movies and can be found with this article online at http://www.cell.com/AJHG/home.

Acknowledgments

We are grateful to the many NM affected individuals and their families, and to their treating physicians, for their participation in this research. Whole-exome sequencing was made possible through the generous support and assistance of David Margulies and the entire staff of The Gene Partnership Project at Boston Children's Hospital. We would like to thank Pankaj Agrawal and Wen-Hann Tan for many helpful discussions during the course of this work. We are thankful to Louise Trakimas of the electron microscope facility at Harvard Medical School for excellent help with zebrafish histology, and the Genotyping and Sequencing Core Facilities at KFSHRC for their technical help. V.A.G. is supported by K01 AR062601 from the National Institute of Arthritis and Musculoskeletal and Skin Diseases of National Institute of Health. This work was also supported by the Muscular Dystrophy Association of USA (MDA201302), National Institutes of Health grant from the National Institute of Arthritis and Musculoskeletal and Skin Diseases R01 AR044345, the AUism Charitable Foundation, and A Foundation Building Strength (to A.H.B.); National Health and Medical Research Council of Australia Early Career Researcher Fellowship #1035955 (to G.R.); Research Fellowship APP1002147 and Project Grant APP1022707(to N.G.L.); the Association Française contre les Myopathies (#15734), Dubai-Harvard Foundation for Medical Research Collaborative Research Grant (to F.S.A.); a UWA Collaborative Research Award (G.R.); and the Great Ormond Street Hospital Children's Charity (to F.M.). E.J.T. and K.S.Y. are supported by University of Western Australia Postgraduate Awards. DNA sequencing was performed by the Boston Children's Hospital Genomics Program Molecular Genetics Core, and confocal microscopy was performed at Boston Children's Hospital Intellectual and Developmental Disability Research Center Imaging Core, both supported by National Institutes of Health grant P30 HD18655. The funders had no role in study design, data collection and analysis, decision to publish, or preparation of the manuscript.

Received: August 9, 2013
Revised: October 15, 2013
Accepted: October 22, 2013
Published: November 21, 2013

Web Resources

The URLs for data presented herein are as follows:

1000 Genomes, http://browser.1000genomes.org
dbSNP, http://www.ncbi.nlm.nih.gov/projects/SNP/
NHLBI Exome Sequencing Project (ESP) Exome Variant Server, http://evs.gs.washington.edu/EVS/
Online Mendelian Inheritance in Man (OMIM), http://www.omim.org/
Picard, http://picard.sourceforge.net/
Pymol, http://www.pymol.org

References

1. Wallgren-Pettersson, C., Sewry, C.A., Nowak, K.J., and Laing, N.G. (2011). Nemaline myopathies. Semin. Pediatr. Neurol. *18*, 230–238.
2. Ryan, M.M., Schnell, C., Strickland, C.D., Shield, L.K., Morgan, G., Iannaccone, S.T., Laing, N.G., Beggs, A.H., and North, K.N. (2001). Nemaline myopathy: a clinical study of 143 cases. Ann. Neurol. *50*, 312–320.
3. Wallgren-Pettersson, C. (2002). Nemaline and myotubular myopathies. Semin. Pediatr. Neurol. *9*, 132–144.
4. Sewry, C.A. (2008). Pathological defects in congenital myopathies. J. Muscle Res. Cell Motil. *29*, 231–238.
5. Hutchinson, D.O., Charlton, A., Laing, N.G., Ilkovski, B., and North, K.N. (2006). Autosomal dominant nemaline myopathy with intranuclear rods due to mutation of the skeletal muscle ACTA1 gene: clinical and pathological variability within a kindred. Neuromuscul. Disord. *16*, 113–121.
6. Pelin, K., Hilpelä, P., Donner, K., Sewry, C., Akkari, P.A., Wilton, S.D., Wattanasirichaigoon, D., Bang, M.L., Centner, T., Hanefeld, F., et al. (1999). Mutations in the nebulin gene associated with autosomal recessive nemaline myopathy. Proc. Natl. Acad. Sci. USA *96*, 2305–2310.
7. Nowak, K.J., Wattanasirichaigoon, D., Goebel, H.H., Wilce, M., Pelin, K., Donner, K., Jacob, R.L., Hübner, C., Oexle, K., Anderson, J.R., et al. (1999). Mutations in the skeletal muscle

alpha-actin gene in patients with actin myopathy and nemaline myopathy. Nat. Genet. *23*, 208–212.

8. Laing, N.G., Wilton, S.D., Akkari, P.A., Dorosz, S., Boundy, K., Kneebone, C., Blumbergs, P., White, S., Watkins, H., Love, D.R., et al. (1995). A mutation in the alpha tropomyosin gene TPM3 associated with autosomal dominant nemaline myopathy. Nat. Genet. *9*, 75–79.
9. Tajsharghi, H., Ohlsson, M., Lindberg, C., and Oldfors, A. (2007). Congenital myopathy with nemaline rods and cap structures caused by a mutation in the beta-tropomyosin gene (TPM2). Arch. Neurol. *64*, 1334–1338.
10. Agrawal, P.B., Greenleaf, R.S., Tomczak, K.K., Lehtokari, V.L., Wallgren-Pettersson, C., Wallefeld, W., Laing, N.G., Darras, B.T., Maciver, S.K., Dormitzer, P.R., and Beggs, A.H. (2007). Nemaline myopathy with minicores caused by mutation of the CFL2 gene encoding the skeletal muscle actin-binding protein, cofilin-2. Am. J. Hum. Genet. *80*, 162–167.
11. Johnston, J.J., Kelley, R.I., Crawford, T.O., Morton, D.H., Agarwala, R., Koch, T., Schäffer, A.A., Francomano, C.A., and Biesecker, L.G. (2000). A novel nemaline myopathy in the Amish caused by a mutation in troponin T1. Am. J. Hum. Genet. *67*, 814–821.
12. Sambuughin, N., Yau, K.S., Olivé, M., Duff, R.M., Bayarsaikhan, M., Lu, S., Gonzalez-Mera, L., Sivadorai, P., Nowak, K.J., Ravenscroft, G., et al. (2010). Dominant mutations in KBTBD13, a member of the BTB/Kelch family, cause nemaline myopathy with cores. Am. J. Hum. Genet. *87*, 842–847.
13. Ravenscroft, G., Miyatake, S., Lehtokari, V.L., Todd, E.J., Vornanen, P., Yau, K.S., Hayashi, Y.K., Miyake, N., Tsurusaki, Y., Doi, H., et al. (2013). Mutations in KLHL40 are a frequent cause of severe autosomal-recessive nemaline myopathy. Am. J. Hum. Genet. *93*, 6–18.
14. Li, H., and Durbin, R. (2009). Fast and accurate short read alignment with Burrows-Wheeler transform. Bioinformatics *25*, 1754–1760.
15. Wang, K., Li, M., and Hakonarson, H. (2010). ANNOVAR: functional annotation of genetic variants from high-throughput sequencing data. Nucleic Acids Res. *38*, e164.
16. Alkuraya, F.S. (2012). Discovery of rare homozygous mutations from studies of consanguineous pedigrees. Curr Protoc Hum Genet. *Chapter 6*, Unit 6, 12.
17. Adams, J., Kelso, R., and Cooley, L. (2000). The kelch repeat superfamily of proteins: propellers of cell function. Trends Cell Biol. *10*, 17–24.
18. Dhanoa, B.S., Cogliati, T., Satish, A.G., Bruford, E.A., and Friedman, J.S. (2013). Update on the Kelch-like (KLHL) gene family. Hum. Genomics *7*, 13.
19. du Puy, L., Beqqali, A., van Tol, H.T., Monshouwer-Kloots, J., Passier, R., Haagsman, H.P., and Roelen, B.A. (2012). Sarcosin (Krp1) in skeletal muscle differentiation: gene expression profiling and knockdown experiments. Int. J. Dev. Biol. *56*, 301–309.
20. Gray, C.H., McGarry, L.C., Spence, H.J., Riboldi-Tunnicliffe, A., and Ozanne, B.W. (2009). Novel beta-propeller of the BTB-Kelch protein Krp1 provides a binding site for Lasp-1 that is necessary for pseudopodial extension. J. Biol. Chem. *284*, 30498–30507.
21. Canning, P., Cooper, C.D., Krojer, T., Murray, J.W., Pike, A.C., Chaikuad, A., Keates, T., Thangaratnarajah, C., Hojzan, V., Marsden, B.D., et al. (2013). Structural basis for Cul3 protein assembly with the BTB-Kelch family of E3 ubiquitin ligases. J. Biol. Chem. *288*, 7803–7814.
22. Spence, H.J., Johnston, I., Ewart, K., Buchanan, S.J., Fitzgerald, U., and Ozanne, B.W. (2000). Krp1, a novel kelch related protein that is involved in pseudopod elongation in transformed cells. Oncogene *19*, 1266–1276.
23. Guerois, R., Nielsen, J.E., and Serrano, L. (2002). Predicting changes in the stability of proteins and protein complexes: a study of more than 1000 mutations. J. Mol. Biol. *320*, 369–387.
24. Lawlor, M.W., Alexander, M.S., Viola, M.G., Meng, H., Joubert, R., Gupta, V., Motohashi, N., Manfready, R.A., Hsu, C.P., Huang, P., et al. (2012). Myotubularin-deficient myoblasts display increased apoptosis, delayed proliferation, and poor cell engraftment. Am. J. Pathol. *181*, 961–968.
25. Kaisto, T., and Metsikkö, K. (2003). Distribution of the endoplasmic reticulum and its relationship with the sarcoplasmic reticulum in skeletal myofibers. Exp. Cell Res. *289*, 47–57.
26. Lu, S., Carroll, S.L., Herrera, A.H., Ozanne, B., and Horowits, R. (2003). New N-RAP-binding partners alpha-actinin, filamin and Krp1 detected by yeast two-hybrid screening: implications for myofibril assembly. J. Cell Sci. *116*, 2169–2178.
27. Paxton, C.W., Cosgrove, R.A., Drozd, A.C., Wiggins, E.L., Woodhouse, S., Watson, R.A., Spence, H.J., Ozanne, B.W., and Pell, J.M. (2011). BTB-Kelch protein Krp1 regulates proliferation and differentiation of myoblasts. Am. J. Physiol. Cell Physiol. *300*, C1345–C1355.
28. Greenberg, C.C., Connelly, P.S., Daniels, M.P., and Horowits, R. (2008). Krp1 (Sarcosin) promotes lateral fusion of myofibril assembly intermediates in cultured mouse cardiomyocytes. Exp. Cell Res. *314*, 1177–1191.
29. Gupta, V., Discenza, M., Guyon, J.R., Kunkel, L.M., and Beggs, A.H. (2012). α-Actinin-2 deficiency results in sarcomeric defects in zebrafish that cannot be rescued by α-actinin-3 revealing functional differences between sarcomeric isoforms. FASEB J. *26*, 1892–1908.
30. Dowling, J.J., Vreede, A.P., Low, S.E., Gibbs, E.M., Kuwada, J.Y., Bonnemann, C.G., and Feldman, E.L. (2009). Loss of myotubularin function results in T-tubule disorganization in zebrafish and human myotubular myopathy. PLoS Genet. *5*, e1000372.
31. Gupta, V.A., Kawahara, G., Myers, J.A., Chen, A.T., Hall, T.E., Manzini, M.C., Currie, P.D., Zhou, Y., Zon, L.I., Kunkel, L.M., and Beggs, A.H. (2012). A splice site mutation in laminin-α2 results in a severe muscular dystrophy and growth abnormalities in zebrafish. PLoS ONE *7*, e43794.
32. Smith, L.S., Beggs, A.H., and Gupta, V.A. (2013). Analysis of skeletal muscle defects in larval zebrafish by birefringence and touch-evoke escape response assays. J. Vis. Exp. *82*, e50925. http://dx.doi.org/10.3791/50925.
33. Zhang, D.D., Lo, S.C., Sun, Z., Habib, G.M., Lieberman, M.W., and Hannink, M. (2005). Ubiquitination of Keap1, a BTB-Kelch substrate adaptor protein for Cul3, targets Keap1 for degradation by a proteasome-independent pathway. J. Biol. Chem. *280*, 30091–30099.
34. Spence, H.J., McGarry, L., Chew, C.S., Carragher, N.O., Scott-Carragher, L.A., Yuan, Z., Croft, D.R., Olson, M.F., Frame, M., and Ozanne, B.W. (2006). AP-1 differentially expressed proteins Krp1 and fibronectin cooperatively enhance Rho-ROCK-independent mesenchymal invasion by altering the function, localization, and activity of nondifferentially expressed proteins. Mol. Cell. Biol. *26*, 1480–1495.

ARTICLE

Mutations in *KLHL40* Are a Frequent Cause of Severe Autosomal-Recessive Nemaline Myopathy

Gianina Ravenscroft,[1,28] Satoko Miyatake,[2,28] Vilma-Lotta Lehtokari,[3,4] Emily J. Todd,[1] Pauliina Vornanen,[3,4] Kyle S. Yau,[1] Yukiko K. Hayashi,[5] Noriko Miyake,[2] Yoshinori Tsurusaki,[2] Hiroshi Doi,[2] Hirotomo Saitsu,[2] Hitoshi Osaka,[6] Sumimasa Yamashita,[6] Takashi Ohya,[7] Yuko Sakamoto,[7] Eriko Koshimizu,[2] Shintaro Imamura,[8] Michiaki Yamashita,[8] Kazuhiro Ogata,[9] Masaaki Shiina,[9] Robert J. Bryson-Richardson,[10] Raquel Vaz,[10] Ozge Ceyhan,[11] Catherine A. Brownstein,[11] Lindsay C. Swanson,[11] Sophie Monnot,[12] Norma B. Romero,[13] Helge Amthor,[12] Nina Kresoje,[14] Padma Sivadorai,[15] Cathy Kiraly-Borri,[16] Goknur Haliloglu,[17] Beril Talim,[17] Diclehan Orhan,[18] Gulsev Kale,[18] Adrian K. Charles,[19] Victoria A. Fabian,[15] Mark R. Davis,[15] Martin Lammens,[20] Caroline A. Sewry,[21] Adnan Manzur,[21] Francesco Muntoni,[21] Nigel F. Clarke,[22] Kathryn N. North,[23] Enrico Bertini,[24] Yoram Nevo,[25] Ekkhard Willichowski,[26] Inger E. Silberg,[27] Haluk Topaloglu,[17] Alan H. Beggs,[11] Richard J.N. Allcock,[14] Ichizo Nishino,[5] Carina Wallgren-Pettersson,[3,4] Naomichi Matsumoto,[2,29,*] and Nigel G. Laing[1,29,*]

Nemaline myopathy (NEM) is a common congenital myopathy. At the very severe end of the NEM clinical spectrum are genetically unresolved cases of autosomal-recessive fetal akinesia sequence. We studied a multinational cohort of 143 severe-NEM-affected families lacking genetic diagnosis. We performed whole-exome sequencing of six families and targeted gene sequencing of additional families. We identified 19 mutations in *KLHL40* (kelch-like family member 40) in 28 apparently unrelated NEM kindreds of various ethnicities. Accounting for up to 28% of the tested individuals in the Japanese cohort, *KLHL40* mutations were found to be the most common cause of this severe form of NEM. Clinical features of affected individuals were severe and distinctive and included fetal akinesia or hypokinesia and contractures, fractures, respiratory failure, and swallowing difficulties at birth. Molecular modeling suggested that the missense substitutions would destabilize the protein. Protein studies showed that KLHL40 is a striated-muscle-specific protein that is absent in *KLHL40*-associated NEM skeletal muscle. In zebrafish, *klhl40a* and *klhl40b* expression is largely confined to the myotome and skeletal muscle, and knockdown of these isoforms results in disruption of muscle structure and loss of movement. We identified *KLHL40* mutations as a frequent cause of severe autosomal-recessive NEM and showed that it plays a key role in muscle development and function. Screening of *KLHL40* should be a priority in individuals who are affected by autosomal-recessive NEM and who present with prenatal symptoms and/or contractures and in all Japanese individuals with severe NEM.

[1]Western Australian Institute for Medical Research and the Centre for Medical Research, University of Western Australia, Nedlands, Western Australia 6009, Australia; [2]Department of Human Genetics, Yokohama City University Graduate School of Medicine, Yokohama 236-0004, Japan; [3]The Folkhälsan Institute of Genetics, Samfundet Folkhälsan, Biomedicum Helsinki, PB 63 (Haartmaninkatu 8), University of Helsinki, Helsinki 00014, Finland; [4]Department of Medical Genetics, Haartman Institute, University of Helsinki, Helsinki 00014, Finland; [5]Department of Neuromuscular Research, National Institute of Neuroscience, National Center of Neurology and Psychiatry, Tokyo 187-8502, Japan; [6]Division of Neurology, Clinical Research Institute, Kanagawa Children's Medical Center, Yokohama 232-8555, Japan; [7]Department of Pediatrics, Odawara Municipal Hospital, Odawara 232-8558, Japan; [8]National Research Institute of Fisheries Science, Yokohama 236-8648, Japan; [9]Department of Biochemistry, Yokohama City University Graduate School of Medicine, Yokohama 236-0004, Japan; [10]School of Biological Sciences, Monash University, Victoria 3800, Australia; [11]The Manton Center for Orphan Disease Research, Genetics and Genomics, Boston Children's Hospital and Harvard Medical School, Boston MA, 02115, USA; [12]Service Génétique Médicale, Hôpital Necker-Enfants Malades, Université Paris Descartes, Paris 75015, France; [13]Unité de Morphologie Neuromusculaire, Institut de Myologie, Institut National de la Santé et de la Recherche Médicale, Paris 75651, France; [14]Lotterywest State Biomedical Facility Genomics and School of Pathology and Laboratory Medicine, University of Western Australia, Perth, Western Australia 6000, Australia; [15]Department of Anatomical Pathology, Royal Perth Hospital, Perth, Western Australia 6000, Australia; [16]Genetic Services of Western Australia, Princess Margaret Hospital for Children and King Edward Memorial Hospital for Women, Subiaco, Western Australia 6008, Australia; [17]Department of Pediatric Neurology, Hacettepe University Children's Hospital, Ankara 06100, Turkey; [18]Department of Pediatric Pathology, Hacettepe University Children's Hospital, Ankara 06100, Turkey; [19]School of Women's and Infants' Health, University of Western Australia, Crawley, Western Australia 6009, Australia; [20]Department of Pathology, University Hospital Antwerp, Antwerp 2650, Belgium; [21]Dubowitz Neuromuscular Centre, UCL Institute of Child Health and Great Ormond Street Hospital for Children, London WC1N 1EH, UK; [22]Institute for Neuroscience and Muscle Research, Children's Hospital at Westmead, Sydney 2145, Australia; [23]Murdoch Childrens Research Institute, The Royal Children's Hospital, Parkville, Victoria 3052, Australia; [24]Unit of Neuromuscular Disorders, Bambino Gesù Children's Hospital, Rome, Lazio 00165, Italy; [25]Neuropediatric Unit, Hadassah Medical Center, Hebrew University of Jerusalem, Jerusalem 91240, Israel; [26]Department of Pediatrics and Pediatric Neurology, University Medicine Göttingen, Göttingen 37075, Germany; [27]Neonatal Intensive Care Unit, Department of Pediatric Research, Women and Children's Division, Oslo University Hospital Rikshospitalet, Oslo 0424, Norway
[28]These authors contributed equally to this work
[29]These authors contributed equally to this work
*Correspondence: nigel.laing@uwa.edu.au (N.G.L.), naomat@yokohama-cu.ac.jp (N.M.)
http://dx.doi.org/10.1016/j.ajhg.2013.05.004.

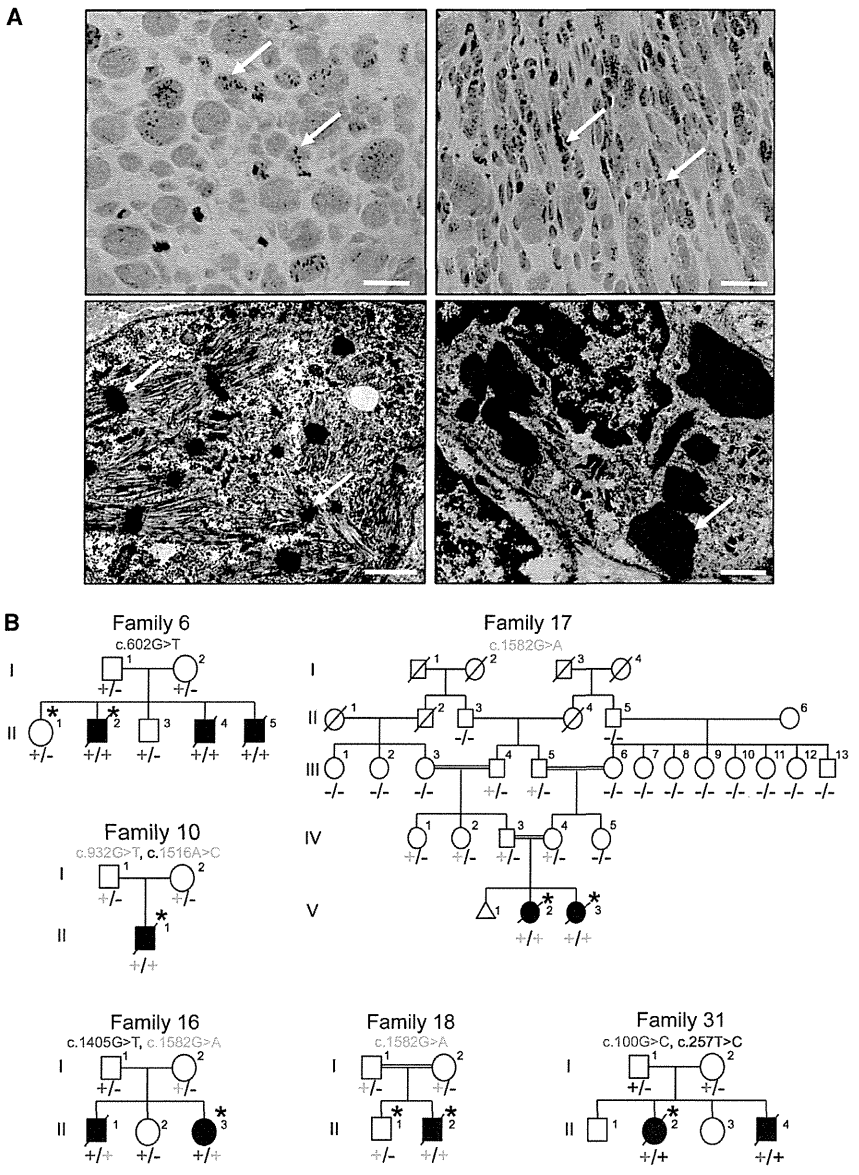

Figure 1. Family Pedigrees and Light and Electron Microscopy of Muscle Biopsies

(A) Modified Gomori trichrome (upper) and electron microscopy (lower) of muscle biopsies from affected individuals of families 15 (right) and 20 (left). Abnormal variation in fiber size, together with many small myofibers and sometimes increased connective tissue, and the presence of numerous red- or purple-stained nemaline bodies (arrows) can be seen (upper panels). Numerous nemaline bodies with varying sizes and shapes and a lack of normal myofibrils are visible by electron microscopy (arrows). Scale bars represent 20 μm for modified Gomori trichrome and 1 μm for electron microscopy.

(B) Pedigrees for the families in which exome sequencing and analysis were performed on the probands. Asterisks indicate the individuals whose DNA was analyzed by exome sequencing. Segregation of the mutations identified in each pedigree is shown.

Introduction

Nemaline myopathy (NEM) is a common form of nondystrophic congenital myopathy and is defined clinically by skeletal-muscle dysfunction and pathologically by the presence of nemaline bodies within myofibers.[1,2] Typical clinical symptoms include hypotonia, muscle weakness of proximal dominance, respiratory insufficiency, and feeding problems. Congenital onset is usual, but a wide variation in age of onset and disease severity is recognized. Mutations in seven genes are known to cause NEM (NEM1–NEM7).[1,2] Six of these encode sarcomere-thin-filament proteins or associated proteins: *ACTA1* (MIM 102610),[3] *CFL2* (MIM 601443),[4] *NEB* (MIM 161650),[5] *TNNT1* (MIM 191041),[6] *TPM2* (MIM 190990),[7] and *TPM3* (MIM 191030);[8] the seventh, *KBTBD13* (kelch-repeat- and BTB-[POZ]-domain-containing 13 [MIM 613727])[9] is involved in the ubiquitin proteasome pathway.[10] Nevertheless, some forms of NEM remain genetically unsolved.

One such subtype, which has long been recognized,[11,12] has apparent autosomal-recessive inheritance and is characterized by severe weakness, in utero presentation of fetal akinesia or hypokinesia and associated abnormalities, and muscle biopsy often showing numerous small nemaline bodies, sometimes only visible by electron microscopy and frequently with virtually no normal myofibrils remaining ("miliary NEM" Figure 1A and Figure S1, available online). We aimed to identify genetic causes of these severe NEM cases by using a combination of linkage analysis, or homozygosity mapping, SNP array, and whole-exome sequencing (WES) in selected families. We have identified loss-of-function mutations in *KLHL40* as a frequent cause of severe NEM and have shown through functional studies that KLHL40 is crucial for myogenesis and skeletal-muscle maintenance.

Subjects and Methods

Subject Details and Ethics

We recruited 143 genetically unresolved severe-NEM-affected families from large congenital-myopathy cohorts in major centers around the world (Boston, Helsinki, Perth, and Tokyo). All individuals within the cohorts were diagnosed with NEM on the basis of muscle-biopsy findings.

Written informed consent was obtained for participation in this study, which was approved by the Human Research Ethics

Committee of the University of Western Australia (UWA), the ethics committee of the Children's Hospital of the University of Helsinki, Yokohama City University School of Medicine, and the Boston Children's Hospital institutional review board. The UWA Animal Ethics Committee approved animal studies.

Microscopy

Light microscopy and electron microscopy of biopsies was performed as previously described.[13]

Whole-Genome SNP Genotyping, Linkage Analysis, and WES

Genotyping was performed for families 6 and 18 with the use of the HumanOmniExpress BeadChip Kit (Illumina) and Infinium II Assay Workflow (Illumina) at the Institute for Molecular Medicine Finland (FIMM). Data were analyzed with PLINK v.1.07. Multiple large homozygous regions were identified, but none included known myopathy-associated genes. WES was performed on one healthy and one affected sibling from family 6 and the proband from family 18 with the SeqCap EZ Human Exome Library v.2.0 exome system (Nimblegen, Roche Diagnostics). Coverage depths were 31- to 62-fold. Variant quantification was performed with the FIMM Variant Calling Pipeline v.1.0 and the Integrative Genomics Viewer (IGV, Broad Institute of MIT and Harvard). All known and heterozygous SNPs were excluded. Healthy siblings' genotypes were used for the exclusion of shared homozygous variants.

Five individuals from family 16 were genotyped with the Human Mapping 10K XbaI 142 2.0 array (Affymetrix) and GeneChip Genotyping Analysis Software (Gtypev4.1). Parametric linkage analysis was performed with Allegro v.2 with a fully penetrant autosomal-recessive model. WES was performed on the proband with the use of the SureSelect Human All Exon 50 Mb Kit (Agilent Technologies) and sequenced in one lane on a GAIIx platform (Illumina) with 108 bp paired-end reads. Reads were aligned to the UCSC Genome Browser (GRCh37/hg19) with Novoalign (Novocraft Technologies). Mean coverage depth was 59-fold. Single-nucleotide variants and small indels were identified with GATK UnifiedGenotyper and filtered according to the Broad Institute's Best Practices guidelines v.3. Variants registered in dbSNP132 were filtered. The filter-passed variants were annotated with ANNOVAR. Only genes with homozygous variants or more than two variants located in the candidate linkage regions were included.

Family 17 was genotyped with the HumanCytoSNP-12 BeadChip (Illumina). MERLIN was used for performing linkage analysis on a subset of 14,514 SNPs.[14] WES was performed for the proband from family 10 and for both siblings from family 17 as described.[15] Coverage depth was 61- to 97-fold. Variants were called with LifeScope 2.5 (Life Technologies) and filtered with ANNOVAR[16] against ENCODE GENCODE v.11 (October 2011 freeze, GRCh37).[17] Two custom variant-filtering steps were used: (1) one against the 1000 Genomes database (February 2012 release) (variants with a minor allele frequency > 0.5% were excluded) and (2) one against the dbSNP135 common database.

Family 31 (BOS74) was one in a cohort of 59 NEM-affected families who underwent WES by the Intellectual and Developmental Disabilities Research Center Core Next-Gen Sequencing Facility of Boston Children's Hospital and Harvard Medical School in collaboration with Axeq Technologies, Complete Genomics, Integrated Genetics (LabCorp), and the Boston Children's Hospital Gene Partnership. Exome sequencing was performed with the Illumina HiSeq 2000 platform. Reads were mapped with the Burrows-Wheeler Aligner (v.0.5.8). SNPs and indels were called with SAMtools (v.0.1.7). Data analysis and variant calling were performed with the Broad GATK Best Practices for identification of SNPs and small indels. Annotated variants were filtered against dbSNP135, the 1000 Genomes Project database (October 2011 edition), and the National Heart, Lung, and Blood Institute (NHLBI) Exome Sequencing Project Exome Variant Server (EVS).

Sequencing

Bidirectional Sanger sequencing of *KLHL40* (RefSeq accession number NM_152393.2) was performed on biobanked DNA from additional probands with severe NEM and their family members in Boston, Helsinki, Perth, Yokohama, and Tokyo. Identified variants were then screened in all available family members. Primer sequences and conditions are available upon request. For detection of the c.1582G>A (p.Glu528Lys) mutation in normal Japanese controls, high-resolution melting (HRM) analysis with and without the spike-in method[18] was performed on LightCycler 480 System II (Roche Diagnostics). If samples showed any aberrant melting patterns, Sanger sequencing was performed for confirmation of the mutation.

LOD Scores

Where possible, MERLIN was used for calculating LOD scores for individual families.[14]

Expression Analysis on Human cDNAs

TaqMan quantitative real-time PCR analyses were performed with cDNAs of human adult (Human MTCPanel I, #636742, Clontech Laboratories) and fetal (Human Fetal MTC Panel, #636747, Clontech Laboratories) tissues.[19] Predesigned TaqMan probe sets for human *KLHL40* (*KBTBD5*, Hs00328078_m1, Applied Biosystems) and human β-actin (*ACTB*, 4326315E, Applied Biosystems) were used. PCR was performed on a Rotor-Gene Q (QIAGEN) (conditions are available upon request) and analyzed with the Rotor-Gene Q Series Software by the $2^{-\Delta\Delta Ct}$ method. Relative concentrations of cDNA were normalized to concentrations obtained from the hearts.

Calculations of the Free-Energy Change upon Amino Acid Substitutions

Molecular structures were drawn with PyMOL. FoldX v.3.0 beta[20] was used through a graphics interface as a plugin for the YASARA molecular viewer.[21] Crystal structures of the kelch domain of human KLHL40 (Protein Data Bank [PDB] code 4ASC) and the BTB (bric-a-brac, tram-track, broad-complex)-BACK (BTB and C-terminal kelch) domain of human KHLH11 (PDB code 3I3N) were energy-minimized with the RepairPDB command implemented in FoldX and subsequently with the BuildModel command for mutagenesis. Protein stabilities were calculated by the Stability command, and the free-energy changes were estimated by subtraction of the free-energy value of the wild-type protein from those of the altered proteins. The procedure was repeated three times for each substitution, and the resultant data were presented as an average value with SDs.

Immunoblotting and Immunohistochemistry

SDS-PAGE and immunoblotting were performed as described.[22,23] For protein studies, C2C12 myoblasts and myotubes were grown and prepared for immunoblotting and immunofluorescence as

described.[23] For KLHL40 immunoblots, the Human Protein Atlas (HPA) rabbit polyclonal KLHL40 (KBTBD5) antibody from Sigma was used (HPA024463 [1:2,500 dilution]). Immunostaining of human and mouse muscle samples was performed as described[13,23] with a KLHL40 antibody (KBTBD5; HPA024463 [1:100 dilution]).

Zebrafish Studies

In Situ Hybridization

Digoxigenin probes for *klhl40a* and *klhl40b* were generated by cDNA amplification of 1,340 and 694 bp sequences, respectively (Table S1). In situ hybridizations were performed as described previously.[24]

Morpholino Microinjection

Antisense translation-blocking morpholinos (Table S1) for *klhl40a* (*klhl40a*-MO) and *klhl40b* (*klhl40b*-MO and *klhl40b*-MO2) were coinjected into 1- to 2-cell-stage embryos at a final concentration of 0.25 or 0.5 mM. Morpholino efficacies were tested by immunoblotting for Klhl40.

Zebrafish Immunohistochemistry

Immunohistochemistry of zebrafish embryos was performed as described[24,25] with myosin heavy chain (MHC) antibody (F59 [1:20 dilution] or A4.1025 [1:10 dilution]; Developmental Studies Hybridoma Bank) and α-actinin (1:100 dilution; Sigma) and filamin C (1:100 dilution; Sigma) antibodies, and Alexa-Fluor-488-conjugated phalloidin (1:100 dilution; Molecular Probes) was used for labeling F-actin. Immunoreactivity was detected with an Alexa-Fluor-594-conjugated anti-mouse secondary antibody diluted in blocking buffer (1:200).

Statistical Analyses

Statistical analyses of clinical features were carried out with SPSS Statistics 19 (IBM) software. Individuals for whom information for a clinical feature was not available were excluded from the analysis of that feature. Either Chi-square tests or Fisher's exact tests were applied for comparing each phenotypic variable between different genotypes. $p < 0.05$ was considered statistically significant.

Results

WES identified homozygous or compound-heterozygous mutations in *KLHL40* (kelch-like family member 40; also known as *KBTBD5* [kelch-repeat- and BTB-(POZ)-domain-containing 5] and *SYRP* [sarcosynapsin]) in six NEM-affected families (families 6, 10, 16–18, and 31; Figure 1B and Table 1). Subsequent screening of *KLHL40* by Sanger sequencing in additional probands with severe NEM resulted in the identification of a total of 19 variants (4 frameshifts, 12 missense mutations, 2 nonsense mutations, and 1 splice site) in 28 (19.6%) apparently unrelated families (Table 1) from the cohort of 143 families affected by severe NEM. In addition, 129 probands with milder NEM were screened, but no *KLHL40* mutations were identified in this cohort, confirming that *KLHL40* mutations are most likely exclusive to cases of severe NEM.

In all cases where it was possible to test unaffected parents, siblings, and extended family, the mutations cosegregated with disease in an autosomal-recessive fashion (Figure 1B), giving a combined LOD score of 5.66 (Table 1). All mutations were either absent from the NHLBI EVS and the 1000 Genomes database[26] or present at low frequencies in the heterozygous state (Table 1). In five additional NEM-affected families, only single *KLHL40* variants were identified (Table S2); the significance of these variants in these individuals remains unclear.

In Japanese persons, *KLHL40* mutations are the most common cause of this severe form of NEM (13/47 [~28%]) as a result of a founder effect with the c.1582G>A mutation. Given that this mutation was present in Turkish, Kurdish, and Japanese families, we completed a haplotype analysis of Japanese and Turkish families (families 16 and 17) but did not identify a common haplotype between them (Figure S2). HRM with confirmatory Sanger sequencing of 510 normal Japanese individuals revealed a heterozygous c.1582G>A mutation in one individual. Therefore, the mutant-allele frequency in the Japanese population was estimated to be 0.0098. According to the equation described by Kimura and Ota[27] and under the assumption of 25 years per generation, the age of this mutation is calculated to be 4,900 years old.

The identified *KLHL40* mutations were scattered throughout all exons (Table 1 and Figure 2A) encoding mostly conserved residues (Figure S3). To investigate disease mechanisms, all substitutions except p.Arg311Leu were mapped to the crystal structures of the kelch domain of human KLHL40 and the BTB-BACK domain of human kelch-like protein 11 (KLHL11; Figures 2B and 2C and Figure S4). p.Arg311Leu (c.932G>T) was predicted to be in the structurally flexible region, a linker of nonconserved amino acids connecting the BACK and kelch domains (Figure S7D), and was therefore excluded from structural consideration. All the modeled substituted residues are involved in intramolecular interactions, and thus the substitutions would most likely destabilize the hydrophobic cores of the BTB-BACK domain (p.Leu86Pro [c.257T>C], p.Val194Glu [c.581T>A], and p.Trp201Leu [c.602G>A]), the kelch domain (p.Pro397Leu [c.1190C>T], p.His455Arg [c.1364A>G], and p.Gly469Cys [c.1405G>T]), the β sheet (p.Thr506Pro [c.1516A>C] and p.Ala538Pro [c.1612G>C]), or the hydrogen bonds between the main chain and side chain (p.Asp34His [c.100G>C] and p.Glu528Lys [c.1582G>A]) or between side chains (p.Glu588Lys [c.1762G>A]) (Figures S5–S7). The p.Pro397Leu and p.Glu588Lys substitutions appear to be conservative for the hydrophobic core and hydrogen bonding, respectively. The former substitution is predicted to affect the polyproline II helix conformation (residues 396–399; Figure S6A). The calculated free-energy change for most substitutions was estimated to be over 2.0 kcal/mol (Figure 2D), which is typically associated with destabilization of domain folds.[28] These analyses suggested that most *KLHL40* missense mutations impair protein stability.

To investigate *KLHL40* expression and KLHL40 abundance, we performed quantitative RT-PCR and immunoblotting of human and mouse tissues. *KLHL40* transcripts

Table 1. ***KLHL40*** **Mutations by Family, Individual LOD Scores, Ethnicity, and Population-wide Incidence**

Family	Exon(s)	Mutation		LOD Score	Ethnicity	Incidence from EVS (1^{st}; 2^{nd})	Incidence from 1000 Genomes (1^{st}; 2^{nd})
		Nucleotide Change	Amino Acid Change				
Family 31[a]	1	c.[100G>C];[257T>C]	p.[Asp34His];[Leu86Pro]	0.6	Vietnamese	ND; ND	ND; ND
Family 2	1	c.[134delC];[134delC]	p.[Pro45Argfs*19];[Pro45Argfs*19]	NA	Italian	NA	ND
Family 3	1	c.[270C>G];[270C>G]	p.[Tyr90*];[Tyr90*]	NA	Turkish	ND	ND
Family 5	1	c.[581T>A];[581T>A]	p.[Val194Glu];[Val194Glu]	0.6	Israeli	ND	ND
Family 6[a]	1	c.[602G>T];[602G>T]	p.[Trp201Leu];[Trp201Leu]	1.454	Turkish	ND	ND
Family 7	1	c.[602G>A];[602G>A]	p.[Trp201*];[Trp201*]	NA	Norwegian	ND	ND
Family 9	1	c.[790delC];[790delC]	p.[Arg264Alafs*59];[Arg264Alafs*59]	0.25	Turkish	NA	ND
Family 10[a]	1 and 4	c.[932G>T];[1516A>C]	p.[Arg311Leu];[Thr506Pro]	NA	Chinese	ND; ND	ND; ND
Family 34	2 and 6	c.[1190C>T];[1762G>A]	p.[Pro397Leu];[Glu588Lys]	NA	Turkish	ND; ND	ND; A = 2 and G = 2,184
Family 12	2 and 4	c.[1270_1272delinsAGATCAAGGT];[1582G>A]	p.[Asp424Argfs*23];[Glu528Lys]	NA	Japanese	NA; ND	ND; ND
Family 13	2 and 4	c.[1281_1294delCTGCCTGGACTCGG];[1582G>A]	p.[Cys428Hisfs*12];[Glu528Lys]	NA	Korean	NA; ND	ND; ND
Family 14	3	c.[1364A>G];[1364A>G]	p.[His455Arg];[His455Arg]	NA	Turkish	ND	ND
Family 15	3	c.[1405G>T];[1405G>T]	p.[Gly469Cys];[Gly469Cys]	NA	Japanese	ND	ND
Family 16[a]	3 and 4	c.[1405G>T];[1582G>A]	p.[Gly469Cys];[Glu528Lys]	0.727	Japanese	ND; ND	ND; ND
Family 17[a]	4	c.[1582G>A];[1582G>A]	p.[Glu528Lys];[Glu528Lys]	1.654	Turkish	ND	ND
Family 18[a]	4	c.[1582G>A];[1582G>A]	p.[Glu528Lys];[Glu528Lys]	0.125	Kurdish	ND	ND
Family 19	4	c.[1582G>A];[1582G>A]	p.[Glu528Lys];[Glu528Lys]	0.25	Kurdish	ND	ND
Family 20	4	c.[1582G>A];[1582G>A]	p.[Glu528Lys];[Glu528Lys]	NA	Japanese	ND	ND
Family 21	4	c.[1582G>A];[1582G>A]	p.[Glu528Lys];[Glu528Lys]	NA	Japanese	ND	ND
Family 22	4	c.[1582G>A];[1582G>A]	p.[Glu528Lys];[Glu528Lys]	NA	Japanese	ND	ND
Family 23	4	c.[1582G>A];[1582G>A]	p.[Glu528Lys];[Glu528Lys]	NA	Japanese	ND	ND
Family 24	4	c.[1582G>A];[1582G>A]	p.[Glu528Lys];[Glu528Lys]	NA	Japanese	ND	ND
Family 25	4	c.[1582G>A];[1582G>A]	p.[Glu528Lys];[Glu528Lys]	NA	Japanese	ND	ND
Family 26	4	c.[1582G>A];[1582G>A]	p.[Glu528Lys];[Glu528Lys]	NA	Japanese	ND	ND
Family 27	4	c.[1582G>A];[1582G>A]	p.[Glu528Lys];[Glu528Lys]	NA	Japanese	ND	ND
Family 28	4	c.[1582G>A];[1582G>A]	p.[Glu528Lys];[Glu528Lys]	NA	Japanese	ND	ND
Family 29	4/5	c.[1608–1G>A];[1608–1G>A]	NA	NA	Turkish	ND	ND
Family 30	5	c.[1612G>C];[1612G>C]	p.[Ala538Pro];[Ala538Pro]	NA	Turkish	ND	ND

The individual pedigree LOD scores are given where possible. This table also shows the incidence of the mutations reported within the NHLBI EVS and the 1000 Genomes browser. Abbreviations are as follows: NA, not available; and ND, not detected.
[a]Families for whom WES was performed.

and their encoded proteins were exclusive to developing and adult skeletal muscle (Figures 3A–3C) and more abundant in fetal muscle than in postnatal muscle (Figure 3C). Confocal microscopy suggested that KLHL40 might localize to the sarcomeric A-band (Figure 3D and Figure S8), a region not previously linked to NEM. Immunoblotting showed that KLHL40 is absent or of low abundance in *KLHL40*-associated NEM muscle (Figure 3E), even for persons harboring two missense mutations (F10 and F17). Immunohistochemistry confirmed that KLHL40 was absent or very scarce in *KLHL40*-associated NEM myofibers (Figure 3F).

We further investigated Klhl40 function in zebrafish. The zebrafish genome contains two orthologs of *KLHL40*: *klhl40a* and *klhl40b*, which have 57% (*klhl40a*) and 55.7% (*klhl40b*) amino acid similarity to human KLHL40. RT-PCR demonstrated expression of both *klhl40* genes at 24 and 48 hr postfertilization (hpf) (Figure S9A). In adult

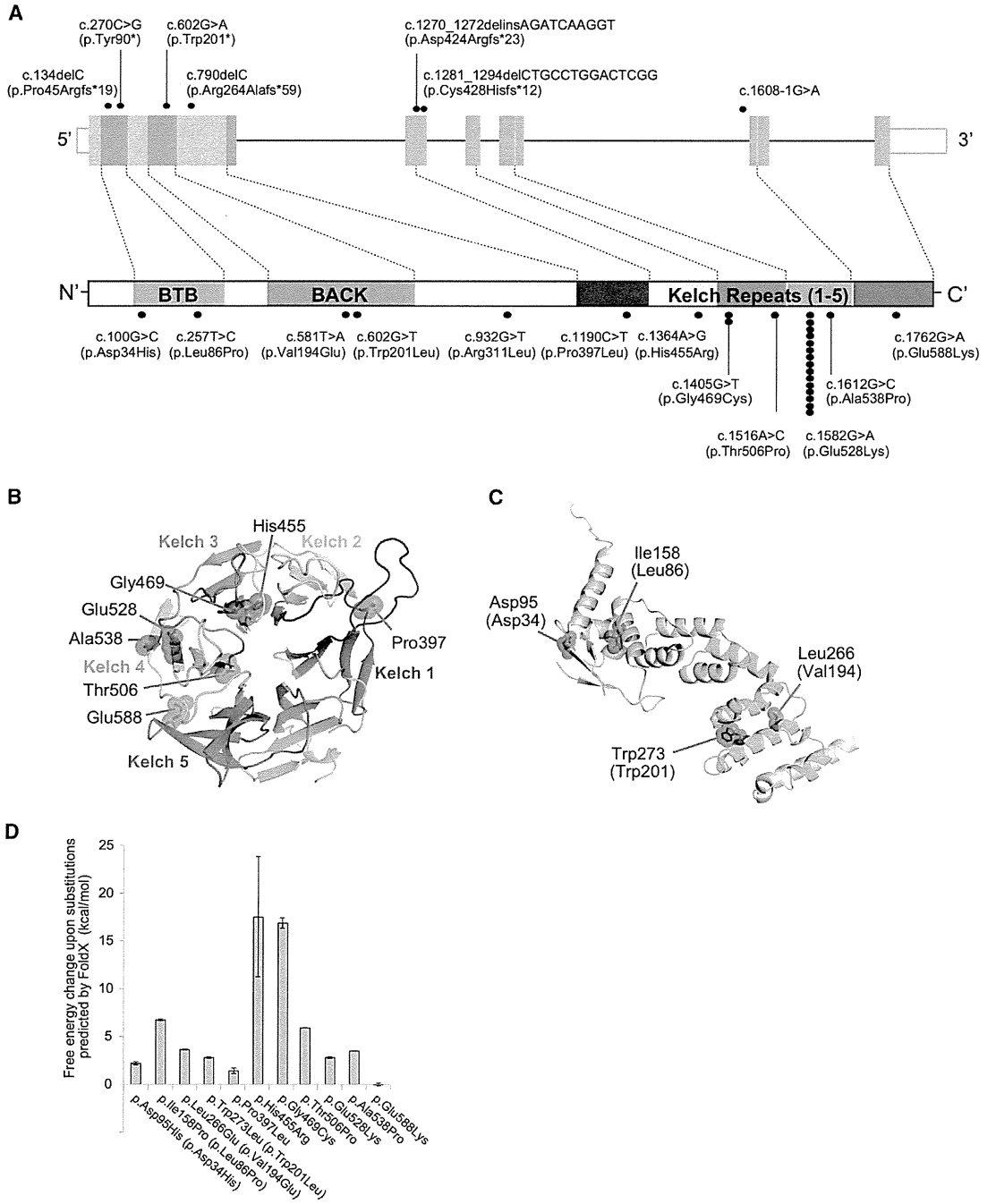

Figure 2. Mutations Identified in Our Cohort and the Structural Modeling of the Missense KLHL40 Substitutions

(A) Schematic presentation of the genomic structure of *KLHL40* (upper) and its encoded protein, KLHL40, with the BTB-BACK domain and kelch repeats (lower). The localization of mutations and substitutions identified is depicted with dots, and the number of dots for each mutation or substitution indicates the number of times it was found. Most substitutions occurred at conserved amino acids. The dots above *KLHL40* indicate truncating mutations, and those below *KLHL40* indicate missense mutations.

(B and C) Structural modeling of the missense KLHL40 substitutions. The crystal structures of the (B) kelch domain of KLHL40 and the (C) BTB-BACK domain of KLHL11 and the location of the substitutions are shown. p.Pro397Leu, p.His455Arg, p.Glu469Cys, p.Thr506Pro, p.Glu528Lys, p.Ala538Pro, and p.Glu588Lys map to the kelch repeats (B), p.Asp34His and p.Leu86Pro map to the BTB domain, and p.Val194Lys and p.Trp201Leu map to the BACK domain (C). The side chains of the mutated residues are shown as sticks with space-filling spheres in red. α helices, β sheets, and loops are drawn as ribbons, arrows, and threads, respectively. Each kelch repeat (B) is color coded in the kelch domain, and the BTB and BACK domains (C) are colored pink and green, respectively. Molecular structures were drawn with PyMOL.

(D) The calculated free-energy changes resulting from the missense substitutions in the kelch domain of human KLHL40 and the BTB-BACK domain of human KLHL11 were predicted by FoldX. Data are presented as the mean ± SD. Residue numbers used in (C) and (D) refer to human KLHL11, and those corresponding to human KLHL40 are in parentheses.

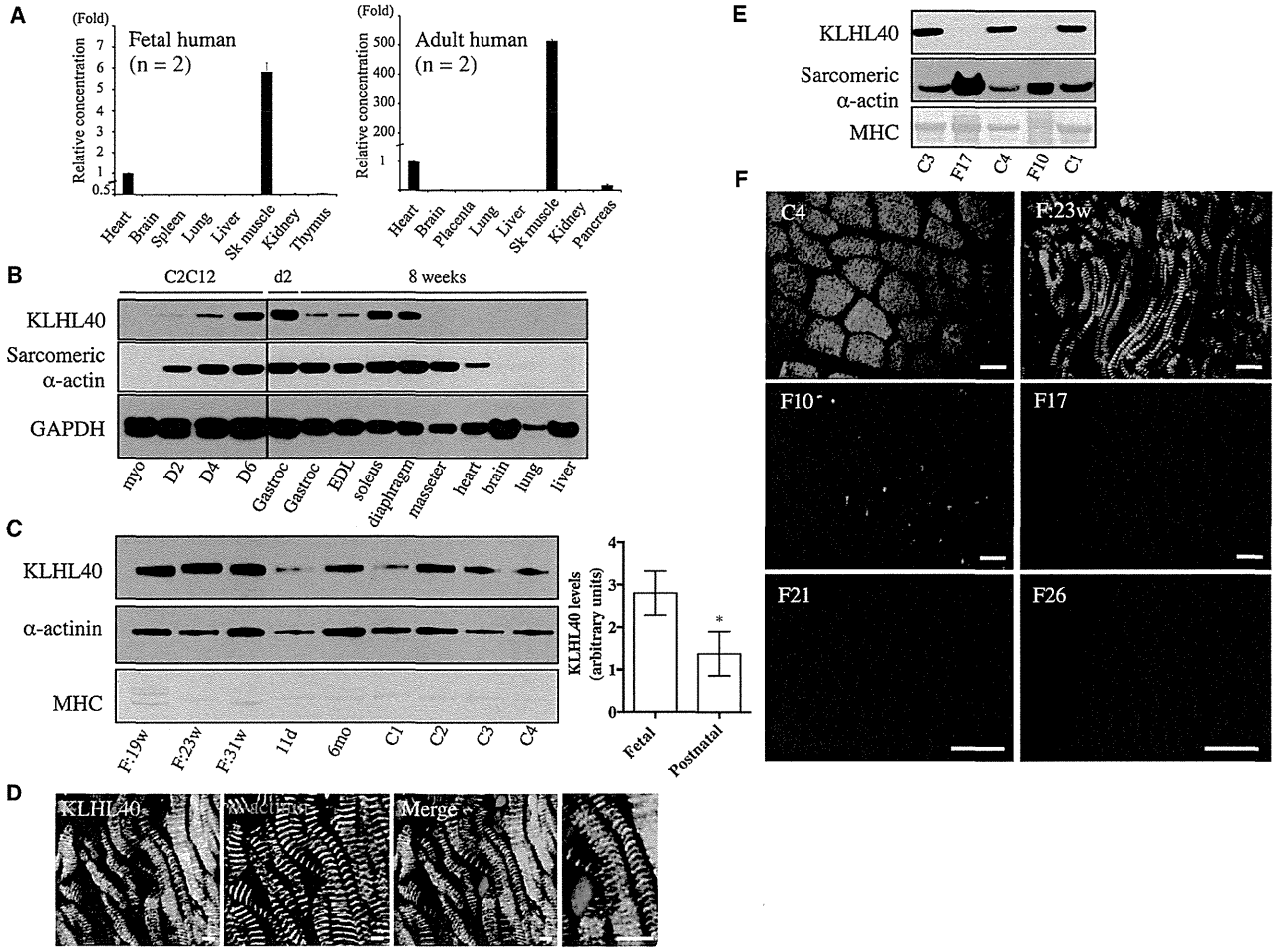

Figure 3. *KLHL40* Expression in Human and Mouse Tissues

(A) Taqman quantitative real-time PCR analysis of cDNA from adult or fetal human tissues. Error bars represent the SD. The following abbreviation is used: Sk, skeletal.

(B) KLHL40 levels in C2C12 cells and mouse tissues (HPA, top panel) and immunoblotting for sarcomeric α-actin (clone 5C5, middle panel) and GAPDH (lower panel). Lanes are as follows: myo, C212 myoblasts; D2, myotubes on day 2 of differentiation; D4, myotubes on day 4 of differentiation; D6, myotubes on day 6 of differentiation; Gastroc (left), C57BL/6 postnatal day 2 (d2) gastrocnemius; Gastroc (right), C57BL/6 8-week-old gastrocnemius; and EDL (extensor digitorum longus) to liver, C57BL/6 8-week-old tissues. For all mouse tissue lysates, samples were pooled from three different mice.

(C) On the left is KLHL40 expression in human skeletal muscle (HPA, top panel), immunoblotting for α-actinin (clone EA-53, middle panel), and Coomassie staining of MHC band (bottom panel). Lanes are as follows: F:19w, 19-week-old fetus; F:23w, 23-week-old fetus; F:31w, 31-week-old fetus; 11d, 11-day-old neonate; 6mo, 6-month-old baby; and C1–C4, healthy adult controls of 19–42 years of age. On the right, KLHL40 intensity normalized to MHC for fetal muscle is 3.34 ± 0.92 (n = 3) versus 1.37 ± 0.21 (n = 6) for postnatal skeletal muscle. *p = 0.023, unpaired two-tailed t test. Error bars represent the SEM.

(D) Single Z-plane confocal microscopy showing localization of KLHL40 (green) and α-actinin (red) in a longitudinal section of skeletal muscle from a 31-week-old fetus; costaining with Hoechst (blue) is also shown (Merge). Scale bars represent 5 μm.

(E) Immunoblotting shows that KLHL40 is absent in *KLHL40*-associated NEM muscle (II-1 from family 10 [F10] and V-2 from family 17 [F17]) compared with healthy control muscle (C1, C3, and C4). Coomassie staining of the MHC band (bottom panel) and immunoblotting for sarcomeric α-actin (clone 5C5, middle panel) indicate similar or greater loading for the *KLHL40*-associated NEM samples compared with control samples.

(F) Immunofluorescence for KLHL40 in a human 23-week-old fetal skeletal muscle sample (F:23w), an adult healthy control (C4), and *KLHL40*-associated NEM muscle biopsies (II-1 from family 10 [F10], V-2 from family 17 [F17], family 21 [F21], and family 26 [F26]). Scale bars represent 50 μm.

zebrafish, *klhl40a* was most abundant in the skeletal muscle and heart and *klhl40b* was most abundant in the skeletal muscle (Figure S9A). At the 16 and 24 hpf stages, expression of both genes was restricted to the muscle precursor cells in the somites (Figure 4A). We knocked down zebrafish *klhl40a* and *klhl40b* with antisense morpholino oligonucleotides (*klhl40a*-MO, *klhl40b*-MO, and *klhl40b*-MO2) (Figures S9B and S10A). Embryos injected with *klhl40a*-MO, *klhl40b*-MO, and *klhl40a*-MO/*40b*-MO (double morpholinos) showed a curved trunk and small head at 48 hpf (Figures 4B and 4C). A normal phenotype resulted from 5 bp mismatched morpholinos (5mis-MOs).